Harmful Algae 148 (2025) 102918

Contents lists available at ScienceDirect

Harmful Algae

journal homepage: www.elsevier.com/locate/hal

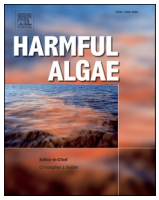

Physiological responses of Arctic and Baltic Sea populations of toxigenic *Alexandrium ostenfeldii* (Dinophyceae) to different climate change stressors

Simon Tulatz [a,*], Urban Tillmann [a], Bernd Krock [a], Jan Tebben [a], Cédric Leo Meunier [b]

[a] Section Ecological Chemistry, Alfred Wegener Institut-Helmholtz Zentrum für Polar- und Meeresforschung, Bremerhaven, Germany
[b] Section Shelf Sea Ecology, Alfred Wegener Institut-Helmholtz Zentrum für Polar- und Meeresforschung, Biologische Anstalt Helgoland, Germany

ARTICLE INFO

Keywords:
Paralytic shellfish toxins
Novel spirolides
15-desmethyl-gymnodimine A
Temperature
Salinity

ABSTRACT

The harmful algal bloom species *Alexandrium ostenfeldii* has a worldwide distribution from polar to tropical habitats and from oceanic to brackish waters. Among other species of the genus *Alexandrium*, it is one of the causative organisms of paralytic shellfish toxins, but additionally, *A. ostenfeldii* has also been shown to produce another class of toxins, cyclic imines. The wide distribution of *A. ostenfeldii* suggests population-specific adaptations to a multitude of environmental parameters and therefore, variable responses to global change drivers, such as warming and shifts in sea surface salinity. In this study we quantified growth and toxin cell quota of two strains of *A. ostenfeldii* isolated from the arctic Kongsfjord and two strains from the northern European Baltic Sea at various temperature conditions, to assess the impact of global warming on locally adapted populations. Overall, growth of the arctic strains was detected at temperatures between 7.5 and 20 °C, with a maximum growth rate at 15 °C for both strains. The two strains from the Baltic Sea revealed intraspecific differences concerning their thermal tolerance. One strain showed no growth at 25 °C, while the other still had a positive growth rate at 27 °C. Furthermore, three of the strains were exposed to salinities between 10 and 40, revealing a tolerance to a broad range of salinities. Neither temperature nor salinity affected the qualitative toxin composition of any strain, but we detected novel cyclic imines in three of the four tested strains. Furthermore, different temperatures and salinities led to dynamic shifts in total toxin cell quota. Additionally, we detected novel spirolides in both arctic strains of *A. ostenfeldii*. These findings suggest that arctic *A. ostenfeldii* might significantly benefit from global warming, while populations from the Baltic Sea may not, and that the Baltic Sea might become unfavourable for western Baltic *A. ostenfeldii* due to climate change driven decreasing salinity in this area.

1. Introduction

The dinoflagellate genus *Alexandrium* has a worldwide distribution and is one of the main genera causing harmful algal blooms (HABs), as it harbours many species able to produce a variety of potent toxins (Anderson et al., 2012). Within this genus, *Alexandrium ostenfeldii,* which was first described as *Goniodoma ostenfeldii* (Paulsen, 1904), has a wide distribution, with reports from cold water arctic regions (Tillmann et al., 2014) to tropical areas (Lim and Ogata, 2005), and from oceanic salinities (Almandoz et al., 2014) to low saline habitats (Hakanen et al., 2012). *A. ostenfeldii* was considered non-toxigenic until the analysis of two cultures from the Danish Limfjord suggested that *A. ostenfeldii* may produce paralytic shellfish toxins (PST), which are responsible for paralytic shellfish poisoning (PSP) (Hansen et al., 1992). PST consist of saxitoxin (STX), one of the most potent natural toxins (Wiese et al., 2010), neosaxitoxin (NEO), gonyautoxins (GTX), their N-sulfocarbamoyl (B- and C-toxins) and decarbamoyl (dc) variants (Krock et al., 2007). PST can accumulate along the food chain and lead to symptoms like paraesthesia, respiratory paralysis, and can lead to death in marine predators and humans when intoxicated seafood is consumed (Anderson et al., 2001; Ching et al., 2015). In addition to PST, *A. ostenfeldii* has also been shown to produce two different groups of cyclic imines (CI), i.e. spirolides (SPX) and gymnodimines (GYM) (Cembella et al., 2000; Van Wagoner et al., 2011). Both, SPX and GYM are regarded as fast-acting neurotoxins, leading to rapid death in mice after intraperitoneal injection (Munday et al., 2012), but no human intoxications have been reported so far, even though these compounds have been detected in higher trophic levels of the marine food webs (Silva et al., 2013).

* Corresponding author.
E-mail address: simon.tulatz@gmx.de (S. Tulatz).

https://doi.org/10.1016/j.hal.2025.102918
Received 7 March 2025; Received in revised form 3 June 2025; Accepted 29 June 2025
Available online 30 June 2025

A. ostenfeldii is thus one of the few HAB species that produces two unrelated classes of toxins. Nevertheless, most *A. ostenfeldii* strains produce either PST (Gu et al., 2013; Kremp et al., 2014), or CI (e.g. Ciminiello et al., 2006; Tillmann et al., 2014), but strains that produce both classes of toxins have also been isolated (Van de Waal et al., 2015; Martens et al., 2016, 2017; Guinder et al., 2018). While the wide geographic distribution of *A. ostenfeldii* suggests a high physiological acclimation potential, variations in toxin profiles are suggested to result from intraspecific genetic differences (Kremp et al., 2019). Beside genetical factors, environmental parameters may play a significant role in shaping the toxin production of harmful algae, and these parameters are of importance concerning climate change. Multiple studies have investigated the influence of environmental parameters on the toxin content of different *Alexandrium* species, but it is often difficult to identify general patterns linking toxin production to individual parameters. For *Alexandrium catenella* and *A. pacificum*, different works have shown that the highest PST cell quota are reached at optimum growth temperatures (Kim et al., 2021; Wang et al., 2022), while opposite results have been reported for another strain of *A. catenella* (Ogata et al., 1987). Similar contrary results have also been published for different *Alexandrium* species grown at different salinities (Lim and Ogata, 2005; Laabir et al., 2013). For the goniodomin-producing species *Alexandrium pseudogonyaulax,* temperature and salinity have a strong influence on the cellular toxin content, while different light and nutrient conditions have not, and toxin cell quota under these conditions are mostly influenced by the growth stage (Möller et al., 2024; Tulatz et al., 2024).

A. ostenfeldii has long been regarded as a background species that often co-occurs with other bloom forming species of the genus *Alexandrium* (Moestrup and Hansen, 1988), but more recent studies have reported increasing occurrences of dense blooms (Kremp et al., 2009; Borkman et al., 2012; Hakanen et al., 2012; Brandenburg et al., 2017; Sildever et al., 2019). As *A. ostenfeldii* is common in a variety of habitats, it is reasonable to suggest that effects of changing environmental parameters are diverse among populations. This has been shown for other planktonic protists and their response to changing temperatures (Boyd et al., 2013), salinities (Kim et al., 2015), and increasingly dissolved CO_2 (Brandenburg et al., 2021). It is therefore necessary to investigate the acclimation potential of different populations to forecast future scenarios concerning geographic expansion, possible bloom formation, and toxicity. The most reasonable and comparable parameter to measure the acclimation potential is growth, as it covers multiple physiological factors.

The aim of the current study was to compare the influence of temperature and salinity conditions on the growth, toxin cell quota, and toxin composition of *A. ostenfeldii* strains from two contrasting ecosystems under anthropogenic and climatic pressure, namely the Baltic Sea and the arctic Kongsfjord. The Baltic Sea is characterized by low and variable salinity that is expected to decrease further in the next decades due to increased freshwater input as a result of climate change (Neumann, 2010; Andersson et al., 2015). Salinity changes coincide with increasing sea surface temperatures, and may influence the local plankton community. The Kongsfjord is characterized by low water temperatures, but the Arctic is experiencing climate change nearly four times as fast as the global average (Rantanen et al., 2022), leading to increased sea surface temperatures, decreased sea surface salinity, and a strengthened stratification of the water column (Karcher et al., 2011). As harmful dinoflagellates may benefit from these changes, e.g. by a prolonged blooming season (Gobler et al., 2017), studies on the autecology of *A. ostenfeldii* are necessary to predict and understand future occurrences and the consequences for marine ecosystems.

2. Material and methods

2.1. Isolation and culture maintenance

Four strains of *A. ostenfeldii* were isolated from water samples taken in the Baltic Sea. While strains W4-B9 and W1-D8 were isolated in 2019 from Wismar (53° 54.57′ N, 11° 26.09′ E), strains K2-A8 and K2-B10 were isolated in 2020 from Kiel (54° 22.14′ N, 10° 09.18′ E). Two strains (4-C4 and 4-F7), were isolated from the Kongsfjord (78° 55.69′ N, 11° 56.07′ E) in Svalbard in summer 2023. All strains were obtained by isolating single cell using a micropipette into 96 well-plates and were kept in half strength K-Medium (K/2) (Keller et al., 1987) without silicate and altered by the replacement of the organic phosphorus source with Na_2HPO_4. The medium was prepared from aged North Sea water with a salinity of 31, sterilized by autoclavation and filtration (0.1 µm, VacuCap filters, Pall Life Sciences, Dreieich, Germany). While the four strains from the Baltic Sea were kept at 15 °C and a salinity of 15, the two arctic strains were cultured at 10 °C and a salinity of 30. Salinities were adjusted through dilution with deionized and purified water (Milli-Q, Millipore, Eschborn, Germany) before the addition of nutrients and the filtration. The pH of the medium was set to 8.0 with 1 M hydrochloric acid and all strains were kept in 70 mL cell culture flasks (TECHNO Plastic Products, Trasadingen, Switzerland) at a photon flux density of 80–100 µmol m^{-2} s^{-1} in a 16:8 h light-dark photocycle.

2.2. Experimental conditions

2.2.1. Temperature experiment

Experiments at different temperatures were performed with both strains from the Kongsfjord and with strains W4-B9 (Wismar) and K2-A8 (Kiel) from the Baltic Sea that were randomly chosen from the Baltic Sea strains, ensuring that both regions were represented. Experimental temperatures were 5, 7.5, 10, 12, 15, 17, 20, 25, 27 and 30 °C. Experiments were performed in K/2 medium at a salinity of 15 for strains W4-B9 and K2-A8, and at a salinity of 30 for strains 4-C4 and 4-F7. For all strains, the photon flux density was adjusted to 80–100 µmol m^{-2} s^{-1} that have been shown to be close to the growth optimum for a strain from Canada (Maclean et al., 2003). Different growth temperatures were obtained by placing the culture flasks into water baths on a temperature-gradient table. Cultures of *A. ostenfeldii* were acclimated to experimental temperatures from the initial temperature of 15 °C for W4-B9 and K2-A8, and 10 °C for 4-C4 and 4-F7. Therefore, *A. ostenfeldii* were stepwise acclimated to higher and lower temperatures in steps of 5 °C, or, if no growth was observed, in steps of 2 °C or 2.5 °C, depending on available temperatures on the temperature gradient table. To quantify growth during acclimation, a subsample of 1 mL was fixed at least once a week with Lugol's iodine at a final concentration of 1 % and cells were counted using an inverted microscope (Axiovert 200 M, Zeiss, Göttingen, Germany). After at least 3 cell divisions, the next acclimation step was performed in the same way. If no increase in cell density was detected during the acclimation phase, the growth rate was regarded as zero and detailed experiments at these conditions were not performed.

After the final acclimation, the experiment was started by dividing the cultures into triplicates with densities of 150–200 cells mL^{-1}. During the experiment, cell densities were determined every second to fourth day, depending on the growth during the acclimation phase, by counting lugol-fixed subsamples with a final concentration of 1 %, using an inverted microscope at magnification x100. The volumes of the subsamples varied between 0.1 and 2 mL, depending on the estimated cell density, to ensure that at least 300 cells per replicate were counted. Specific growth rates µ (d^{-1}) were calculated as $N_t=N_0$ $exp^{\mu t}$ using exponential regression of a number of selected time points in the exponential growth phase. For a better comparison of the whole "growth rate versus temperature curves" of the tested strains, temperature optimum range that allows high growth rates for each tested strain was defined as 75 % of the maximum growth rate, calculated with the best fitting polynomial regression using the Dynamic Fit Wizard (SigmaPlot, Systat Software Inc., Düsseldorf, Germany) through all data points where growth was observed.

Samples for CI and PST analysis (see 2.3.) were taken at two time points (Fig. 1). Since the onset of the stationary phase and the maximum

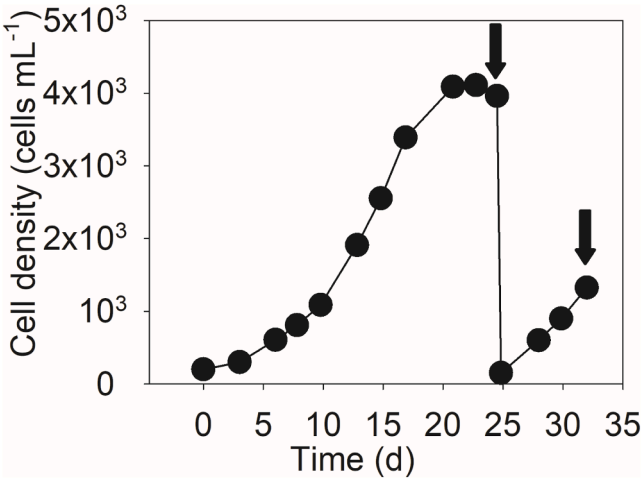

Fig. 1. Sampling scheme for the temperature and salinity experiments. Arrows show time points where samples for toxin analysis and cell volumes were taken. First arrow indicates the stationary growth phase, 2nd arrow indicates the exponential growth phase.

cell density under the current experimental conditions were not known in advance, the following sampling strategy was implemented to ensure that the exponential phase would be captured at cell densities adequate for toxin analysis: The first sampling was performed in the stationary growth phase, i.e. when no further increase in cell density was detected for at least 2 consecutive sampling points. Subsequently, the culture flasks were refilled with fresh medium, resulting in densities between 100 and 200 cells mL^{-1}, and the second sampling was performed at a density of about 1000 cells per mL when cells were in the exponential growth phase. Strain 4-C4 was only sampled in the stationary growth phase at 17 °C, as no growth was detected after refilling the culture flasks. At both sampling points, the pH of the cultures was measured (EcoScan pH 5, EUtech Scientific Engineering, Aachen, Germany), and cell sizes were measured using lugol-fixed subsamples that were viewed at x200 magnification under an inverted microscope directly after. The length and width of at least 35 cells per replicate were measured using a digital camera (Axiovert, Zeiss) and the Axiovision software (Zeiss). Cell volume was calculated assuming rotational ellipsoid cells, using the formula $\pi/6\ d^2\ L$ with d being the diameter an L the length of the cell.

2.2.2. Salinity experiment

For the salinity experiment, media with different salinities < 31 were prepared by dilution of North Sea water with deionized and purified water. Salinities > 31 were obtained by the addition of commercial sea salt (Sea Salts S9883, Sigma Aldrich). Both, deionized water and sea salt were added in advance of the medium-preparation filtration step. Before the start of the experiments, strains W4-B9, K2-A8 and 4-C4 were adapted to salinities of 7.5, 10, 15, 20, 30, 35, 40, and 45. Therefore, cultures of the originally salinity 15 for strains W4-B9 and K2-A8 (30 for 4-C4) were first transferred to salinities 10 and 20 (25 and 35 for strain 4-C4). After at least three cell divisions, subcultures were further transferred stepwise to the next lower or upper salinity, and this procedure was repeated with acclimated subcultures until all salinities were available. When no growth was detected during the acclimation by cell counts of lugol-fixed subsamples, these conditions were excluded from the experiments. Salinity was measured with a conductivity meter (SB80PC, VWR sympHony Meters, Hannover, Germany). The experiment was performed in triplicates at 15 °C in K/2 medium at a photon flux density of 80–100 µmol $m^{-2}\ s^{-1}$ with a starting cell density of 150–200 cells mL^{-1}. Cell densities and size were determined as described above (2.2.1.). Cells for the analysis of CI and PST were harvested in the exponential and the stationary growth phase (2.3.). Strain 4-F7 died during the acclimation at every condition with no identifiable reason and was therefore excluded from the experiments.

2.3. Toxin analysis

2.3.1. Cell harvest and toxin extraction

During the exponential growth phase and the stationary phase, duplicates of 25–30 mL of culture, one for the analyses of CI and one for PST measurements, were transferred into 50 mL centrifugation tubes and centrifuged at 3220 x *g* and 10 °C for 10 min (model 5810R, Eppendorf, Hamburg, Germany). The supernatants were discarded and the cell pellets were transferred to 2 mL cryovials (Sarstedt micro tube, Nümbrecht, Germany), and centrifuged again at 16,000 x g for 5 min (Eppendorf 5415). The remaining supernatant was carefully removed with a pipette and each tube was filled with 0.9 g lysing matrix D (Thermo-Savant, Illkich, France) and either 250 µL of UPLC grade methanol for the extraction of CI, or with the same volume of 0.03 M acetic acid for the extraction of PST. The cells were lysed by reciprocal shaking in a homogenizer (FastPrep-24, MP Biomedicals, Eschwege, Germany) at 6.5 m s^{-1} for 45 s. After another centrifugation step at 10 °C and 16,000 x *g*, the supernatant was transferred to a spin filter with a pore size of 0.45 µm (Millipore, Eschborn, Germany). The samples were spin filtered for 30 s at 845 x g. The filtrate was transferred to autosampler vials and stored at −20 °C until measurements by liquid chromatography coupled to tandem mass spectrometry (LC-MS/MS) for CI, or liquid chromatography with fluorescence detection (LC-FLD) for PST.

2.3.2. LC-MS/MS conditions for the detection of cyclic imines

LC-MS/MS measurements for spirolides and gymnodimines were performed on a liquid chromatograph (1100 LC, Agilent, Waldbronn, Germany), coupled to a triple-quadrupole mass spectrometer (Sciex 4000 QTrap, Applied Biosystems, Darmstadt, Germany). Reversed-phase (RP) chromatography was performed on a C_8 column (50×2 mm), packed with 3 µm Hypersil (Phenomenex, Aschaffenburg, Germany) thermostated at 25 °C. For the gradient elution, two eluents were used with eluent A being water and eluent B being methanol:water (95:5, v:v), both buffered with 50 mM formic acid and 2 mM ammonium formate. Total run time for each sample was 30 min, consisting of a linear gradient from 5 % B to 100 %B within 10 min, isocratic elution with 100 % B for 10 min, return to initial conditions within 1 min and 9 min of column equilibration at 5 % B. Injection volume was 5 µL at a constant flow rate of 200 µL min^{-1}

Parameters of the MS/MS were as follows: Ion-Spray-Voltage: 5500 V, temperature: 650 °C, nebulizer gas: 40 psi, auxiliary gas: 70 psi, declustering potential: 121 V; entrance potential: 10 V, exit potential: 22 V, curtain gas: 20 psi. Measurements were performed in the selected reaction monitoring (SRM) in the positive mode, measuring 45 different transitions (Table 1).

Detected spirolides and gymnodimines were quantified against external standards of SPX 1 and GYM A (Certified reference material, NRC, Halifax, Canada) with concentrations of 100, 200 and 500 pg μL^{-1}, using the software Analyst (version 1.5, Applied Biosystems). Spirolides and gymnodimines of which no standards are available are given as SPX 1 or GYM A equivalents. Collision induced dissociation (CID) spectra for the identification of spirolides and gymnodimines were recorded, using the same conditions.

2.3.3. HR-MS/MS

Unknown CIs were further analysed by Ultra-High-Performance Liquid Chromatography (UHPLC) coupled to a high-resolution mass spectrometer (Q-Exactive Plus, both Thermo Fisher Scientific, Schwerte, Germany). Chromatography was performed on a C18 column (C18 BEH, 50 × 2 mm, 1.7 µm particle size, equipped with guard-column, Thermo Fisher Scientific) at 32 °C. Eluents consisted of A: ultrapure water, and B: acetonitrile, both containing 10 mM ammonium formate and 0.1 % formic acid. The gradient program was as follows: 10 % B for 0.5 min, followed by a linear gradient to 100 % B within 6.5 min and held for 3

Table 1
Mass transitions of the measured compounds in the SRM. SPX=spirolide, GYM=gymnodimine.

Precursor ion> fragment ion (*m/z*)	Compound	Precursor ion> fragment ion (*m/z*)	Compound
722 > 164		678 > 164	13,19-didesmethyl-SPX C
722 > 180		678 > 150	
720 > 164		674 > 164	
720 > 150		670 > 164	
718 > 164		668 > 164	
710 > 150		666 > 180	
710 > 164		666 > 164	
708 > 164	SPX D	658 > 164	
708 > 180	27-hydroxy-13-desmethyl-SPX C	652 > 164	SPX I
706 > 164	SPX C, 20-methyl-SPX G	650 > 164	SPX H
706 > 150		640 > 164	
704 > 164		618 > 164	
698 > 164		592 > 164	
696 > 164	20-hydroxy-13,19-didesmethyl-SPX D	582 > 564	
694 > 164	Desmethyl-SPX D	548 > 530	
694 > 150	SPX B	542 > 524	
694 > 180	27-hydroxy-13,19-didesmethyl-SPX C	526 > 508	GYM E
692 > 164	13-desmethyl-SPX C (SPX1), SPX G	524 > 506	GYM D
692 > 150	SPX A	522 > 504	12-methyl-GYM A
692 > 178	27-oxo-13,19-didesmethyl-SPX C	510 > 492	Desmethyl-GYM D
692 > 180		508 > 490	GYM A
690 > 164		494 > 476	Desmethyl-GYM A
686 > 164			

min. After that, the column was equilibrated with 10 % B for 1 min. The flow rate was 0.55 mL min^{-1}. The effluents of the first 0.6 min of each measurement were discarded to avoid salt deposits. Positive Ion Calibration Solution (Pierce, Thermo Fisher Scientific) was used for the calibration of the instrument. The source parameters for all MS experiments were as follows: Capillary temperature 266 °C, auxiliary gas 400 °C, spray voltage 3.5 kV, sheath gas flow 51, and auxiliary gas rate 18. Resolution of the MS was 280,000 (*m/z* 200). The scan range was 100 to 1000 m/*z*. Molecular assignment of the $[M + H]^+$ ions were accepted when within the mass tolerance range of the instruments error (<1 ppm). The Xcalibur software package (Thermo Electron Corporation) was used to export exact mass lists, intensity, noise level and resolution to individual peak lists.

2.3.4. Analysis of paralytic shellfish toxins

LC-FLD was performed on a liquid chromatograph (LC1100, Agilent) coupled to a post column derivatisation system (PCX 2500, Pickering Laboratories, Mountain View, CA, USA). Separation of analytes was reached, using a RP column (Luna C_{18}, 250×4.6 mm, Phenomenex, Aschaffenburg, Germany), packed with particles with a 5 μm diameter, kept at 20 °C. For the elution, two eluents were used, with eluent A: 6 mM 1-octanesulfonic acid and 6 mM 1-heptanesulfonic acid in 40 mM ammonium phosphate, adjusted to pH 7 with phosphoric acid and 0.75 % tetrahydrofuran, and eluent B: 13 mM 1-octanesulfonic acid 50 mM phosphoric acid, set to pH 7 with ammonium hydroxide, 15 % acetonitrile (v:v) and 1.5 % tetrahydrofuran. Total run time was 45 min, consisting of 15 min isocratic elution with 100 % A, followed by change to 100 % B and 20 min isocratic elution with 100 % B. Subsequently, eluent composition returned to initial conditions within 1 min, followed by 9 min of column equilibration. Injection volume for each sample was 20 μL and chromatography was performed at a constant flow of 1 mL min^{-1}. Eluates were continuously oxidized in a reaction coil heated to 50 °C with 10 mM periodic acid in 550 mM ammonium hydroxide at a flow rate of 0.4 mL min^{-1} and subsequently acidified with 0.75 M nitric acid at a flow rate of 0.4 mL min^{-1} and 20 °C. Paralytic shellfish toxins were detected by a dual monochromator fluorescence detector with an excitation wavelength (λ_{ex}) of 333 nm and an emission wavelength (λ_{em}) of 395 nm. Detected PST were identified and quantified against an external standard mix, containing saxitoxin, neosaxitoxin, decarbamoyl-saxitoxin, gonyautoxins 1–4, and decarbamoyl-gonyautoxin-2/3 (Certified reference material, NRC, Halifax, Canada).

2.4. Phylogenetic analysis

Cells of all strains were harvested in the exponential growth phase as mentioned in 2.3.1. Extraction of genomic DNA and amplification of the D1/D2 region of the large (28S) subunit (LSU) was performed as described in Tillmann et al. (2022). The PCR products were purified using the NucleoSpin Gel and PCR clean-up kit (Macherey-Nagel). Sequencing of the PCR product of the four strains from the Baltic Sea was performed as described in (Tillmann et al., 2017), the LSU sequences of the two strains from the Kongsfjord were sequenced by Eurofins (Eurofins Genomics Germany GmbH).

Sequences obtained in this study and 37 further sequences of *A. ostenfeldii* available at GenBank (Table S1) were used for the phylogenetic analysis. One strain of *A. tamarense* was used as an outgroup to root the phylogenetic tree. LSU sequences of all strains were aligned using MAFFT (Multiple Alignment with Fast Fourier Transform) version 6.864 with default settings. Bayesian interference (BI) was calculated with the program Mr. Bayes version 3.2.7 (Ronquist et al., 2012), using the GTR+*G* model. Two runs of four chains, containing three heated and one cold, were performed for 50×10^6 generations and no prior knowledge about the data was assumed. Trees were sampled every 5000th generation and for each run the first 25 % of samples were declared as the burn-in phase and therefore discarded. Furthermore, Maximum Likelihood (ML) analysis with all sequences was performed using PhyML version 3.1 (Guindon et al., 2010) and the GTR model. Bootstrap (BS) values were calculated from 1000 replicates.

2.5. Statistical analysis

To compare the means of the different strains, a two-way ANOVA was performed. For pairwise comparisons, the Holm-Sidak post-hoc test with adapted significance levels was performed. To analyse means of different treatments within one strain, a Kruskal-Wallace one-way ANOVA on ranks with a Student-Newman-Kewls test for pairwise comparisons was used. To further explore connections between different variables, Pearson Product Moment Correlations were conducted. Differences were regarded significant at a p-value <0.05. All statistics were performed with SigmaPlot 11 (Systat Software Inc., Düsseldorf, Germany)

3. Results

3.1. Phylogenetic analysis

Bayesian and Maximum Likelihood analysis of the LSU rDNA resulted in almost identical phylogenetic trees. The two strains from the Kongsfjord, 4-C4 and 4-F7, grouped together with strains from Western Greenland. Iceland and the Western North-Atlantic (Fig. 2). The strains isolated from Kiel grouped together with strains isolated from the North Sea or adjacent fjords, e.g. from Norway, Scotland and Denmark. Both strains from Wismar formed a subclade with two strains from Ireland, the United Kingdom, and Spain, in a large clade with other strains from the Baltic Sea, e.g. from Finland and Poland.

Fig. 2. Phylogenetic tree made from the LSU D1/D2 sequences of *A. ostenfeldii*. Bold Strains were sequenced in this study. *A. tamarense* was used as an outgroup to root the tree. Numbers at the nodes give the posterior probability of the bayesian interference and the bootstrap values from the ML analysis (BI/BS). Bootstrap values are only shown when >50.

3.2. Temperature experiment

3.2.1. Growth responses

Overall, positive growth rates were detected at temperatures between 7.5 and 27 °C (Fig. 3). Strain W4-B9 from Wismar was the only strain growing at temperatures above 23 °C and even reached maximum growth rates of 0.27 d^{-1} at 25 °C, while the optimum range for this strain was from 18.6 to 26.8 °C. Acclimation at 10 and 12 °C led to a decrease in cell density by about 50 % within 20 days. The same decrease in cell density was observed within 6 days at 30 °C (Supplement, Figure S1a). On the other hand, no significant differences between the growth rates at 23, 25, and 27 °C of strain W4-B9 were detected, but these growth rates were significantly higher than growth rates at lower temperatures ($p < 0.05$). The Kiel strain K2-A8 grew at temperatures between 10 and 23 °C, with a maximum growth rate of 0.18 d^{-1} at 20 °C and an optimum range from 14.6 to 22.2 °C. Growth rates of strain K2-A8 differed significantly from each other at all tested temperatures ($p < 0.05$). During acclimation at 5 and 7.5 °C, no growth but relatively constant cell densities were detected, while at 25 and 27 °C cell densities decreased (Figure S1b). Strain 4-C4 from the Kongsfjord showed a temperature tolerance shifted to lower temperatures and was the only strain with growth at 7.5 °C, but no growth was detected at temperatures above 17 °C. Maximum growth for this strain of 0.23 d^{-1} was detected at 15 °C and was closer to the maximum temperature than to the minimum temperature. All other growth rates were significantly lower ($p < 0.05$). The optimum range of strain 4-C4 was from 11.8 to 15.9 °C. During acclimation at 5 and 20 °C, only very slow growth occurred within 20 days, followed by a rapid decrease in cell density (Figure S1c). The second arctic strain 4-F7 had positive growth between 10 and 20 °C with an optimum range between 11.0 and 19.0 °C and the highest growth rate at 15 °C (0.20 d^{-1}). For strain 4-F7 growth rates at all tested temperatures were significantly different from each other ($p < 0.05$). Acclimation at 5 and 7.5 °C led to constant cell densities, at 23 °C a reduction of about 70 % was observed (Figure S1d).

Comparisons of the growth responses of the four tested strains at different temperatures showed that strain W4-B9 differed significantly from all other strains ($p_{W4\text{-}B9/K2\text{-}A8}<0.001$, $p_{W4\text{-}B9/4\text{-}C4}<0.001$, $p_{W4\text{-}B9/4\text{-}F7}=0.005$) while no significant differences between the other strains were detected.

Different temperatures also influenced the maximum cell densities of all strains. These ranged from 787 to 5940 cells mL^{-1}, and the highest cell density was always detected in connection with the respective maximum growth rate (Table S2). Furthermore, treatments also had an effect on the cell volumes of the four strains in both growth phases. Cell

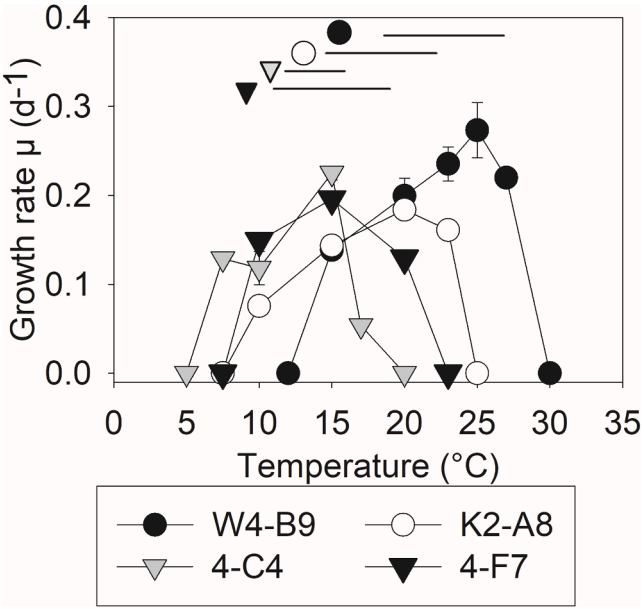

Fig. 3. Growth rates of the four tested strains at different temperatures. $n = 3$ ± 1SD. Horizontal lines represent the calculated optimum ranges.

volumes of all strains ranged from about 10000 to 20000 μm³ in both growth phases, with strain W4-B9 having the smallest cells in the majority of measurements. A significant negative Pearson correlation was detected between growth rate and cell volume in the exponential growth phase for strains K2-A8 ($p = 0.002$) and 4-C4 ($p = 0.008$).

3.2.2. Toxin composition

Temperature treatments had no effect on the qualitative toxin profile of any strain. W4-B9 from Wismar produced exclusively PST in both growth phases and no CI were detected (see table S3 for limits of detection). STX was the major compound at all temperatures, followed by C1/C2, B1, and GTX2/3 (Fig. 4). Furthermore, a significant increase of STX with rising temperatures was detected ($p < 0.001$) that correlated negatively with a decrease of C1/C2 ($p = 0.003$), and also with B1 ($p = 0.02$).

K2-A8 from Kiel only produced CI while PST were not detected above detection limits (Table S3). The two major toxins produced by this strain were SPX 1 and 13,19-didesmethyl-SPX C, making up approximately 95 % of total detected CI (Fig. 5). Minor CIs were GYM A, 27-hydroxy-13-desmethyl-SPX C, 15-desmethyl-GYM A, and the undescribed compound (Cp) 3 that displays characteristic mass spectrometric features of SPX (Table 2), with 60, 25, 10, and 5 % of the minor compounds, respectively (Figure S2). The two arctic strains 4-C4 and 4-F7 had qualitatively nearly identical toxin compositions. For both strains, the major compounds SPX C and 20-methyl-SPX G making up about 95 % of the total toxins at all temperatures and both growth phases. Minor compounds of these strains were SPX 1, and some other not further characterized Cp 1–5 (Table 2, Figure S2) that form fragments of m/z 164 and 180 that are typical for spirolides. Minor compounds of strain 4-C4 were composed of 64 % SPX 1, 22 % Cp 1, 8 % Cp 2, 2 % Cp 3, and 5 % Cp5, while Cp 4 was not detected in strain 4-C4. The relative composition of the minor SPX of strain 4-F7 consisted of 46 % SPX 1, 27 % Cp 4, 22 % Cp 1, 2 % Cp 2 and Cp 3, and 1 % Cp 5. Furthermore, strain 4-F7 responded with a significant increase of the relative amount of SPX C at higher temperatures ($p < 0.05$) (Fig. 5).

3.2.3. Toxin quotas

PST cell quota of strain W4-B9 ranged from 10.8 to 23.1 fmol cell^{-1} (3.8–8.4 pg cell^{-1}) and from 14.0 to 23.8 fmol cell^{-1} (4.7–8.6 pg cell^{-1}) in the exponential and the stationary growth phase respectively (Fig. 4). In the exponential growth phase, toxin quotas were highest at 15 and 27 °C, and significantly higher than the minimum at 23 °C ($p_{15/23}$=0.013, $p_{27/23}$=0.026). Furthermore, a positive correlation between cell volume and PST cell quota in the exponential growth phase was detected ($p = 0.015$). The highest cell quota during the stationary phase was measured at 15 °C but no significant differences to other temperatures were detected.

Total CI cell quota of strain K2-A8 ranged from 56.5 to 96.5 fmol cell^{-1} (39.2–67.0 pg cell^{-1}) in the exponential growth phase (Fig. 5a). The highest cell quota was detected in samples at 10 °C and was significantly higher than cell quota at all other temperatures ($p < 0.01$). The lowest cell quota was detected at 20 °C but differed significantly only from cell quota at 10 °C. Cell quotas in the exponential growth phase showed a positive correlation with cell volume and a negative correlation to growth rate ($p < 0.05$). In the stationary growth phase, the highest CI cell quota was also measured at 10 °C with 104.1 fmol cell^{-1} (72.2 pg cell^{-1}) and the lowest at 20 °C with 32.6 fmol cell^{-1} (22.8 pg cell^{-1}) (Fig. 5b). In the stationary growth phase, cell quotas differed significantly between all temperatures ($p < 0.05$) and correlated positively with cell volume in the stationary growth phase ($p = 0.01$). Total cell quotas of CI for strain 4-C4 showed only minor changes in the exponential growth phase, ranging from 109.1 fmol cell^{-1} (76.9 pg

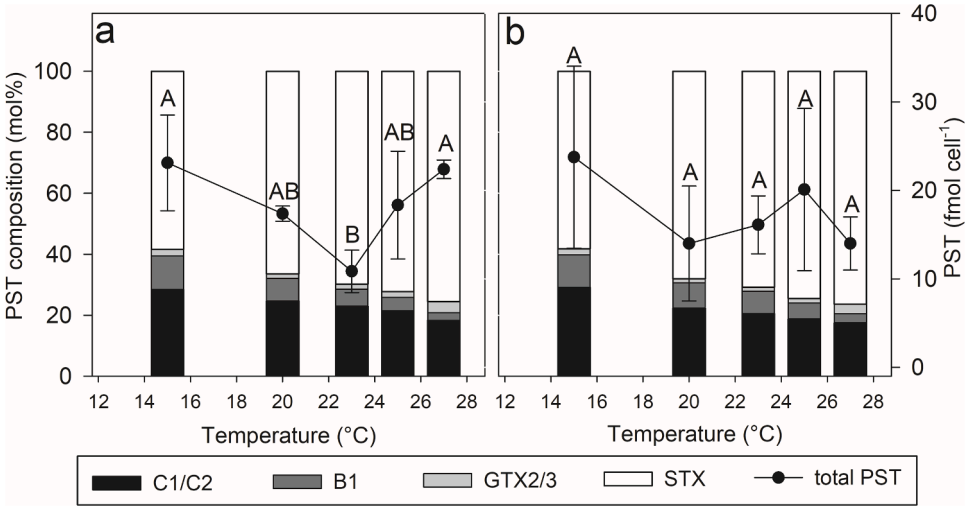

Fig. 4. PST composition and total PST cell quota of strain W4-B9 at different temperatures. a: exponential growth phase, b: stationary growth phase. Different capitals indicate significant differences between total PST cell quotas at different temperatures ($p \leq 0.05$).

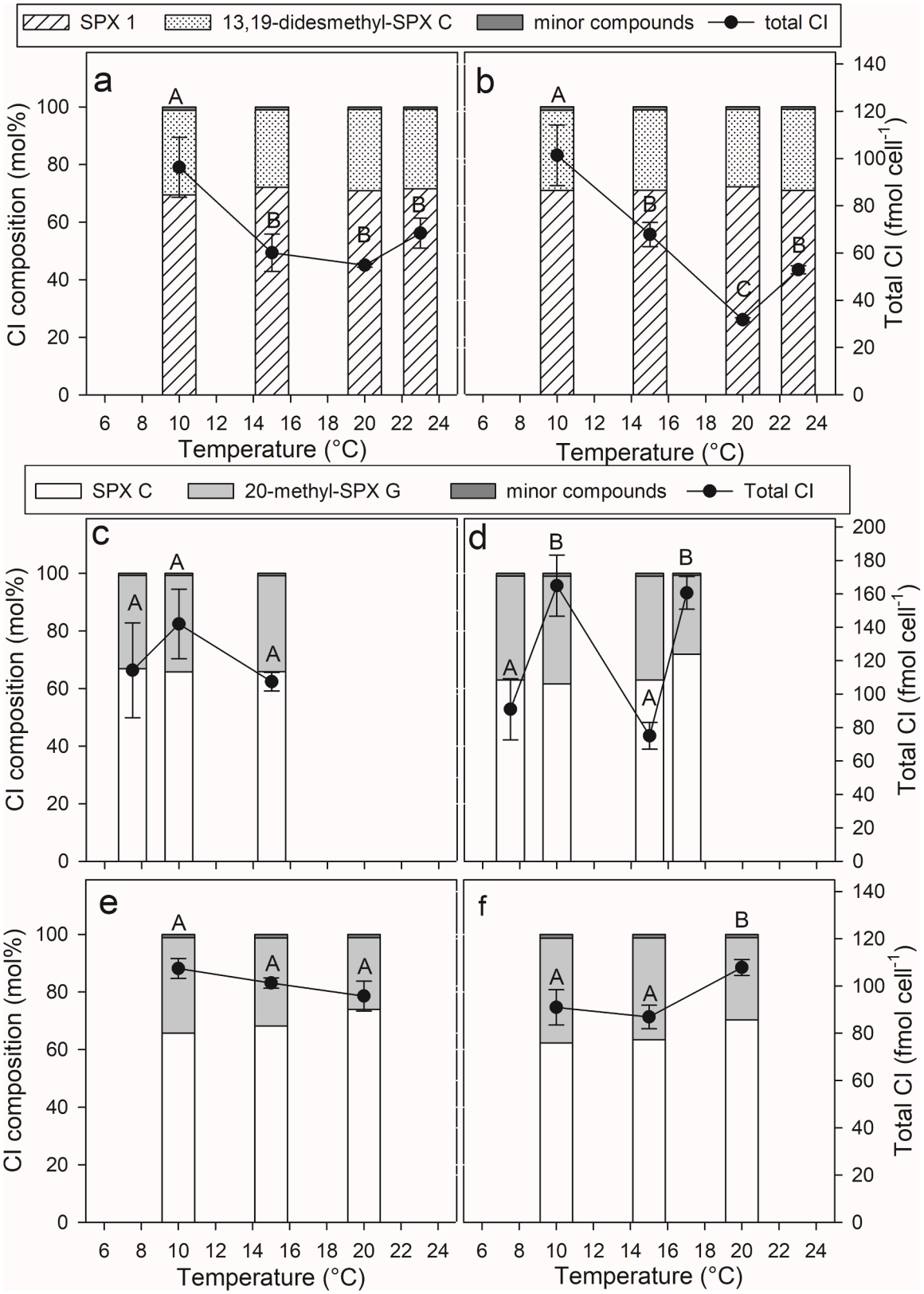

Fig. 5. Total cyclic imine cell quota and CI composition of the strains K2-A8 (a, b), 4-C4 (c, d), and 4-F7 (e, f) at different temperatures. a, c, *e* = exponential growth phase, b, d, *f* = stationary growth phase. Different capitals indicate significant differences between total CI cell quotas at different temperatures ($p \leq 0.05$).

Table 2
Percentage composition of detected CI in the temperature and salinity experiments covering all growth phases. Bold numbers represent major compounds and give the percentage of total CI. Normal numbers represent minor compounds and give the percentage only of all minor compounds. Numbers in parenthesis = Standard deviation; –= not detected.

Compound	Q1/Q3 (*m/z*)	Retention time (min)	K2-A8	4-C4	4-F7
SPX 1 (13-desmethyl-SPX C)	692/164	10.9	**71.8 (1.4)**	63.5 (6.6)	46.0 (2.9)
SPX C	706/164	11.0	–	**66.5 (5.1)**	**67.3 (4.4)**
20-methyl-SPX G	706/164	11.4	–	**32.5 (5.1)**	**31.5 (4.3)**
13,19-didesmethyl-SPX C	678/164	10.5	**27.2 (1.4)**	–	–
27-hydroxy-13-desmethyl-SPX C	708/180	11.1	25.2 (19.6)	–	–
Cp1	690/164	12.53	–	22.2 (5.4)	21.6 (2.5)
Cp2	722/180	11.3	–	8.4 (5.7)	1.8 (1.7)
Cp3	710/164	10.5	5.3 (1.9)	1.5 (0.6)	2.2 (0.4)
Cp4	720/164	11.4	–	–	27.6 (2.7)
Cp5	722/180	11.6	–	4.8 (2.6)	0.7 (0.6)
GYM A	508/490	10.0	59.5 (14.7)	–	–
15-desmethyl-GYM A	494/476	9.6	10.0 (3.5)	–	–

cell^{-1}) at 15 °C to 144.1 fmol cell^{-1} (97.6 pg cell^{-1}) at 10 °C, but differences were non-significant (Fig. 5c), but correlated negatively with the specific growth rate ($p = 0.008$). In the stationary growth phase, total CI was more variable ranging from 76.1 to 167.1 fmol cell^{-1} (53.7–115.4 pg cell^{-1}) at 15 and 10 °C respectively (Fig. 5d). Cell quotas at 10 and 17 °C were significantly higher than cell quota at 7.5 and 15 °C ($p \leq 0.001$). For strain 4-F7, a linear, but non-significant decrease in CI cell quota from 109.1 fmol cell^{-1} (76.9 pg cell^{-1}) at 10 °C to 97.3 fmol cell^{-1} (68.8 pg cell^{-1}) at 20 °C was observed (Fig. 5e). In the stationary growth phase, CI cell quotas ranged from 92.5 to 109.4 fmol cell^{-1} (62.2–77.1 pg cell^{-1} (Fig. 5f), with a significantly higher cell quota at 20 °C compared to 10 and 15 °C ($p < 0.01$), and a positive correlation to cell volume in the stationary growth phase ($p = 0.01$).

3.3. Salinity experiment

3.3.1. Growth responses

Overall, salinities from 7.5 to 45 were tested, and growth was detected in a salinity range from 10 to 40. Strain W4-B9 from Wismar had positive growth rates between salinity 10 and 30, with a maximum of 0.16 d^{-1} at salinity 20 that was significantly higher than growth at other salinities ($p < 0.05$), and an optimum range from salinity 13.7 to 27.8 (Fig. 6). Acclimation at salinity 35 led to a decrease in cell density by about 60 % within 6 days (Figure S3a). Acclimation at salinities 5 and 7.5 resulted in 25 % and 5 %, respectively, of deformed or disrupted cells directly after the start of the trial (Figure S4), followed by a rapid decline in cell density at salinity 5 and no growth at salinity 7.5 (Figure S3a). Strain K2-A8 from Kiel had a maximum growth rate at salinity 25 with 0.17 d^{-1}, but no significant differences of the growth rates between salinity 15 and 35 were detected. At salinities 10 and 40 the growth rates decreased significantly compared to the maximum ($p < 0.05$). The optimum range for this strain was between salinity 15.6 to 34.2. While acclimation at salinity 45 led to a slow decrease in cell density, at salinities 5 and 7.5, the decline in cell density was rapid (Figure S3b). Strain 4-C4 from the Kongsfjord was the only strain that did not grow at salinity 10. A maximum growth rate of 0.23 d^{-1} was detected at salinity

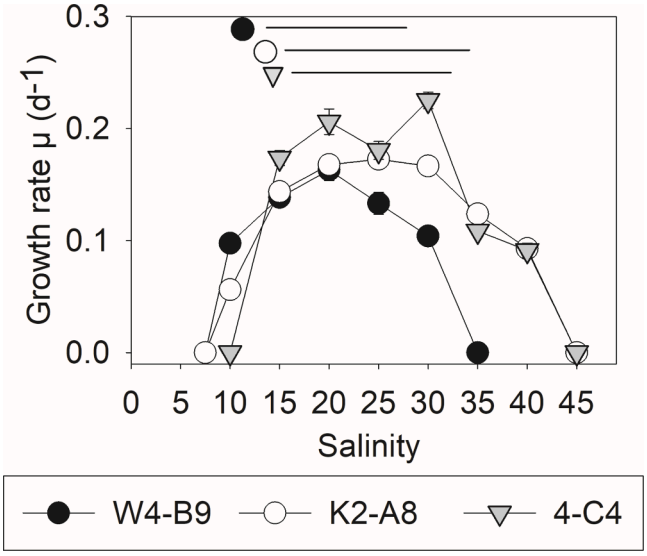

Fig. 6. Growth rates of the three tested strains at different salinities. $n = 3 \pm$ 1SD. Horizontal lines represent the calculated optimum ranges.

30 and was significantly higher that all other growth rates of this strain ($p < 0.05$). The lowest growth rate was measured at a salinity of 40 and the optimum range was from salinity 16.3 to 32.3. While an acclimation at salinity 45 led to no cell density changes, a trial at salinity 10 led to a rapid decline in cell density (Figure S3c). A strain comparison revealed significant differences in growth response at different salinities between all tested strains ($p_{W4\text{-}B9/K2\text{-}A8}$=0.033, $p_{W4\text{-}B9/4\text{—}C4}$<0.001, $p_{K2\text{-}A8/4\text{—}C4}$=0.011).

Cell densities in the stationary growth phase ranged from 924 to 2750 mL^{-1} for strain W4-B9, from 940 to 4180 mL^{-1} for K2-A8 and from 1785 to 5940 mL^{-1} for 4-C4 (Table S4). Cell volumes of all strains ranged from 12000 to 21000 μm^3 and from 9000 to 24000 μm^3 in the exponential and stationary growth phase respectively, with a significant negative Pearson correlation between growth rate and cell volume for strain K2-A8 ($p = 0.003$).

3.3.2. Toxin composition

The strains exposed to different salinities did not produce other toxins than those mentioned in section 3.1.2. Strain W4-B9 had a significant relative increase of STX at high salinities in the stationary growth phase ($p < 0.05$), accompanied with a relative decrease of C1/C2 (Fig. 7). Strain K2-A8 had a stable toxin composition at all salinities in both growth phases with SPX 1 and 13,19-didesmethyl SPX C adding up to about 95 % of all toxins (Fig. 8). The toxin composition of strain 4-C4 always consisted of over 95 % of SPX C and 20-methyl-SPX G and low amounts of minor compounds (Fig. 8), but the portion of SPX C increased significantly at high salinities.

3.3.3. Toxin quotas

The PST cell quotas of strain W4-B9 ranged from 22.0 to 37.8 fmol cell^{-1} (7.9–13.9 pg cell^{-1}) and from 20.2 to 41.9 fmol cell^{-1} (7.2–15.6 pg cell^{-1}) in the exponential growth phase and the stationary growth phase, respectively (Fig. 7). In both growth phases, cell quotas at salinity 10 were significantly higher than at all other salinities ($p \leq 0.01$), but no differences between higher salinities were detected. In both growth phases, PST cell quota correlated positively with cell volumes ($p < 0.01$).

A comparable pattern of toxin cell quota dynamics was detected in strain K2-A8 from Kiel (Fig. 8a, b). In both growth phases, maximum CI cell quotas were detected at a salinity of 10, with 127.3 and 116.1 fmol cell^{-1} (87.2 and 79.7 pg cell^{-1}) in the exponential and stationary growth phase, respectively, that were significantly higher than cell quota at higher salinities ($p \leq 0.001$). At salinities between 15 and 40, cell quotas

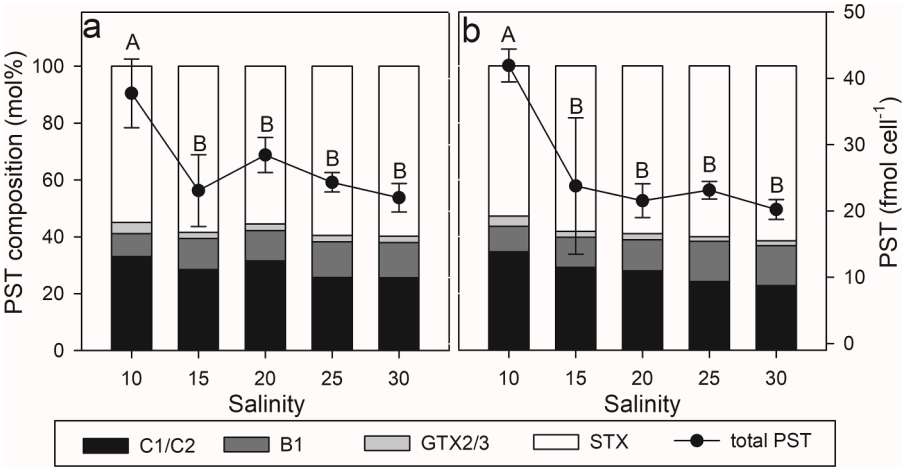

Fig. 7. PST composition and total PST cell quota of strain W4-B9 at different salinities. a: exponential growth phase, b: stationary growth phase. Different capitals indicate significant differences between total PST cell quotas at different salinities ($p \leq 0.05$).

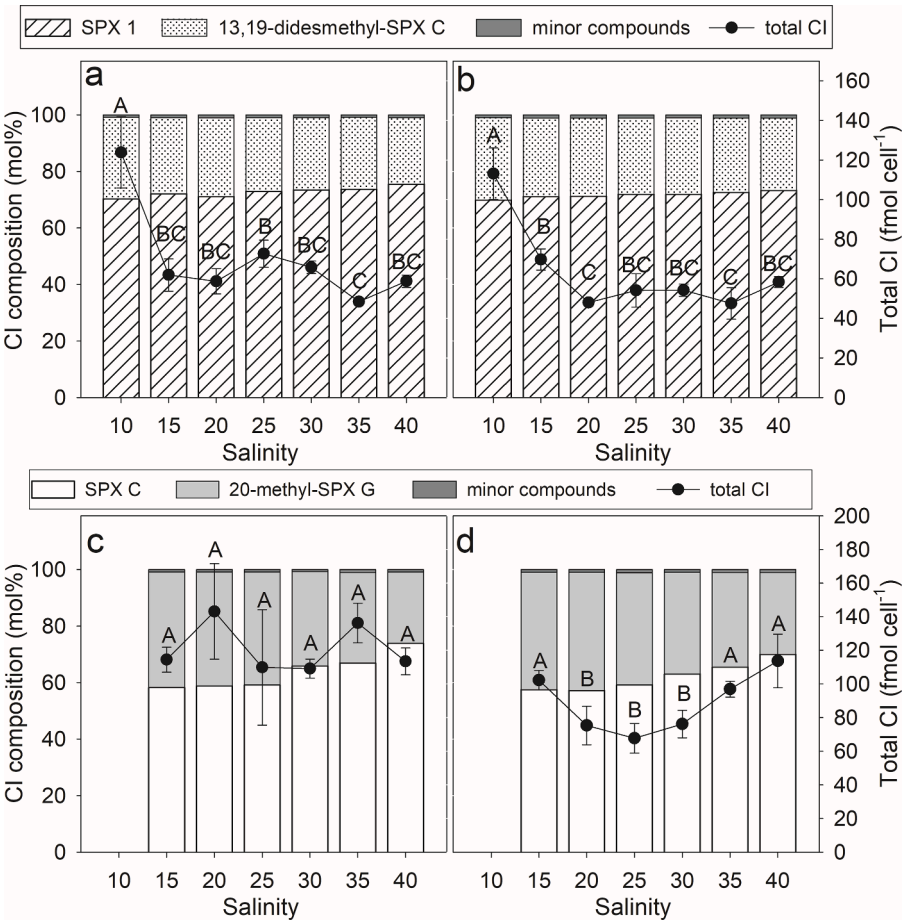

Fig. 8. Total cyclic imine cell quota and CI composition of the strains K2-A8 (a, b) and 4-C4 (c, d) at different salinities. a, c = exponential growth phase, b, d = stationary growth phase. Different capitals indicate significant differences between total CI cell quotas at different salinities ($p \leq 0.05$).

were subject to small, but partly significant variations ($p < 0.05$). CI cell quotas of the exponential growth phase had a significant negative correlation to growth rates, and in both growth phases a positive correlation to cell volume ($p < 0.05$). The CI cell quotas of strain 4-C4 varied from 109.1 to 145.2 fmol cell^{-1} (76.9–102.6 pg cell^{-1}) in the exponential growth phase (Fig. 8c). Differences between salinities were non-significant, but a positive correlation to cell volume was detected ($p = 0.003$). In the stationary growth phase, cell quotas ranged from 68.8 to 115.3 fmol cell^{-1} (48.4–81.3 pg cell^{-1}) (Fig. 8d). Cell quotas at intermediate salinities of 20, 25, and 30 were significantly lower than cell quotas at salinities 15, 35, and 40 ($p < 0.05$).

4. Discussion

4.1. Growth responses

4.1.1. Comparison of Arctic and Baltic A. ostenfeldii strains

The two strains, K2-A8 and W4-B9, from the Baltic Sea seem to be well adapted to the present temperature conditions of their origin. Growth rates were highest at 20 and 25 °C, respectively, and the sea surface temperature in southern parts of the Baltic Sea averages 18 °C in summer, but regularly exceeds 20 °C (Siegel et al., 2006). Similar optimum temperatures have also been reported for other dinoflagellates from northern Europe, e.g. *Tripos* spp., *Gymnodinium aureolum, Karlodinium veneficum,* and *Alexandrium pseudogonyaulax* (Nordli, 1957; Nielsen and Tønseth, 1991; Nielsen, 1996; Tulatz et al., 2024). Furthermore, similar temperatures have been described during *A. ostenfeldii* blooms in the northern Baltic Sea (Hakanen et al., 2012), suggesting that these temperatures support near optimal growth in the Baltic Sea.

In contrast, an adaption of the two strains from the Kongsfjord to the present temperature regime in their geographic origin appears not to be the case. Both strains from the Kongsfjord did not grow at temperatures below 7.5 °C. This is particularly noteworthy, as the Kongsfjord rarely reaches temperatures above 8 °C in the summer (Fischer et al., 2024). Notably in this respect is that the Kongsfjord is subject to "atlantification", the inflow of warmer Atlantic water (Smoła et al., 2017). It is therefore possible that the local population of *A. ostenfeldii* is not specifically adapted to low temperatures but was introduced with Atlantic water at a historically relative short time span. In accord with this hypothesis, the phylogenetic analysis of these two strains revealed that they group together with other strains from the North Atlantic, but also with strains from the west coast of Greenland, which also is influenced by Atlantic Water. Even though an exact extrapolation to their origin is not possible, phylogeny seems to support the Atlantic origin of the two strains from Kongsfjord. As the plankton community of the Kongsfjord has regularly been studied (Hasle and Heimdal, 1998; Okolodkov et al., 2000; Seuthe et al., 2011; Caroppo et al., 2017; Bhaskar et al., 2020), but *A. ostenfeldii* is either rarely detected or not identified to species level, this further indicates that it does not reach high densities in this area. For other toxigenic species of the genus *Alexandrium*, e.g. *A. catenella*, massive blooms in high latitude areas have been reported (Anderson et al., 2021), suggesting that this species is established in arctic areas, but blooms of *A. ostenfeldii* in arctic regions have not been reported. However, as the Artic is warming more than three times as fast as the global average (Rantanen et al., 2022), and increases in surface temperatures of up to 6 °C have been predicted for the year 2100 (Pachauri et al., 2014), climate change could favour a permanent establishment of *A. ostenfeldii* in high latitudes.

A comparison with other protistan species from the Arctic showed that many diatoms are specifically well adapted to low growth temperatures; for example, for *Chaetoceros* sp. and *Nitzschia frigida* growth was detected at −1.8 °C (Suzuki and Takahashi, 1995) and *Fragillariopsis cylindrus* grow well at 1 °C (Pančić et al., 2015). For other plankton groups, the abundant arctic flagellate *Micromonas* sp. likewise grows well at 0 °C (Lovejoy et al., 2007) and, among dinoflagellates, *Protoceratium reticulatum* from Western Greenland have positive growth rates at 0 °C (Sala-Pérez et al., 2016). However, a further increase in water temperature in high latitude areas, combined with atlantification could alter the local plankton communities, by introducing, and favouring the permanent establishment of new species.

Besides temperature, salinity is another important factor shaping plankton communities and regulating growth and geographical expansion of species. The distribution of *A. ostenfeldii* as well at oceanic salinities like the North Atlantic (Gribble et al., 2005) and the Mediterranean Sea (Ciminiello et al., 2006), as in brackish waters (Kremp et al., 2009; Martens et al., 2016) suggests a tolerance to a wide range of salinities of this species. Both strains from the Baltic Sea had positive growth rates at salinities as low as 10, but lower salinities led to disrupted cells and cell death. This is particularly interesting as *A. ostenfeldii* from the northern-eastern Baltic Sea is reported to grow at salinities as low as 3 (Kremp et al., 2009). These findings suggest that the Baltic Sea is inhabited by multiple populations of *A. ostenfeldii*. However, with average salinities of 13 and 16 in Wismar and Kiel respectively (Feistel et al., 2010; Gräwe et al., 2013), and the suggestion that the Baltic Sea salinity will decrease by about 2 units by the year 2100 (Neumann, 2010; Andersson et al., 2015), this might inhibit the growth of *A. ostenfeldii* not adapted to low salinities in the southern Baltic Sea. Furthermore, even small decreases in salinity might allow the northern Baltic *A. ostenfeldii* populations that are well adapted to low salinities and moreover capable of forming intense high-density blooms to expand their distribution range to the southern Baltic Sea. While *A. ostenfeldii* from the Baltic Sea have to be able to grow at low salinities, for strains from the Kongsfjord an ecological need for coping with low salinity in not obvious but nevertheless its growth maximum is at salinities below that of its origin. Strain 4-C4 did not grow at salinity 10, but at salinity 15 growth was already close to the maximum (Fig. 6). Strains of *A. ostenfeldii* from marine areas of higher salinities have been reported to be able to grow at low salinities, but growth rate is usually reduced (Maclean et al., 2003; Suikkanen et al., 2013). The tolerance of strain 4-C4 to relatively low salinities might be an adaption to shifts in sea surface salinity due to melting sea ice and glaciers in the arctic summer, but it may also be a widely spread species characteristic. While long-term monitoring of the Kongsfjord showed that the salinity at the origin of strain 4-C4 usually does not decrease below salinity 30 (Fischer et al., 2024), the salinity of arctic fjords has been suggested to decrease by about 0.12 per year (Sejr et al., 2017). These climate change driven processes would, however, not affect *A. ostenfeldii* in the Kongsfjord due to the tolerance to low salinities of this population.

4.1.2. Differences between the Baltic sea strains

Significant overall differences in growth at different temperatures between the Baltic Sea strains that have been isolated about 100 km apart from each other, were obvious (Fig. 3). The growth vs temperature curve of the western strain K2-A8 with a maximum growth rate at 20 °C and a steep decrease at higher temperatures is similar to one reported for an *A. ostenfeldii* strain from the Limfjord in northern Denmark (Jensen and Moestrup, 1997). In contrast, the growth curve of the more eastern strain W4-B9 from Wismar was clearly shifted to higher temperatures. A further increase of the Sea surface temperatures of the Baltic Sea due to global warming thus might benefit the PST producing strain W4-B9. A connection between PST producing *A. ostenfeldii* and high temperatures has also been suggested for *A. ostenfeldii* from the north-eastern Baltic Sea (Tahvanainen et al., 2012), but more data are needed to evaluate if all PST-producing strains of *A. ostenfeldii* generally tolerate higher temperatures.

On an annual scale, the temperature of the Baltic Sea is subject to seasonal changes, while the salinity of the southern Baltic Sea is relatively stable (Omstedt and Axell, 2003), averaging 13 and 16 in Wismar and Kiel, respectively (Feistel et al., 2010; Gräwe et al., 2013). For *A. ostenfeldii*, it is suggested that the salinity tolerance depends on the origin of the strain and therefore the native salinity (Suikkanen et al., 2013). Both strains from the Baltic Sea had the same tolerance to low salinities, with growth detected at salinity 10, but not at 7.5. However, only the western strain K2-A8 but not the eastern strain W4-B9 had positive growth rates at salinities above 30. With this salinity tolerance strain K2-A8 resembles a strain isolated from the brackish Limfjord (Jensen and Moestrup, 1997). While strain W4-B9 is not able to sustain oceanic salinities, a distinct adaption to low salinities, as it is obvious for *A. ostenfeldii* strains from the northern Baltic Sea (Suikkanen et al., 2013), is also not achieved.

The physiological differences between strains K2-A8 and W4-B9 suggest distinct genetic differences between the two strains as well, as it has been described for the diatom *Skeletonema marinoi* (Sjöqvist et al.,

2015) and for the common mussel *Mytilus edulis* (Väinölä and Hvilsom, 1991) from the transition zone from the North Sea to the Baltic Sea. Phylogenetic analysis of the two strains from the Baltic Sea indeed show that they are grouped in different clades (Fig. 2). While the eastern strain W4-B9 groups together with other strains from the low haline Baltic Sea but also with strains from brackish ponds and estuaries from the North Sea in one main clade, the western strain K2-A8 is located in the other main clade with strains from the North Sea and adjacent fjords, but also with strains from the North Atlantic. Hence, we hypothesize that the origin of strain K2-A8 is the North Sea or the polyhaline transition zone between the North Sea and the Baltic Sea, while the origin of strain W4-B9 might be in the eastern or northern parts of the Baltic Sea. A spreading of dinoflagellates from the North Sea or the polyhaline Kattegat into the meso- and oligohaline waters of the Baltic Sea has previously been described e.g. for *A. pseudogonyaulax* (Kremp et al., 2019) and *Prorocentrum cordatum* (Hajdu et al., 2000) and it is therefore possible that the Kiel population of *A. ostenfeldii* is another example for this. Furthermore, low-salinity-adapted populations of various plankton species like *Peridiniella catenata* (Gromisz and Witek, 2001), *Protoperidinium* spp. (Hällfors et al., 2013), and *A. ostenfeldii* (Suikkanen et al., 2013) proliferate in the low saline parts of the Baltic Sea and an expansion of their geographical ranges must also be considered.

4.2. Toxin cell quotas of A. ostenfeldii

Temperature and salinity did not only alter growth dynamics of the tested strains, but also led to shifts in toxin cell quotas. CI cell quotas of the strains K2-A8 from Kiel, 4-F7, and 4-C4 from the Kongsfjord ranged from 34 to 115 pg cell^{-1}, revealing that all three strains have very high cell quotas compared to other strains that usually range between 1 and 20 pg cell^{-1} (Otero et al., 2010; Medhioub et al., 2011; Suikkanen et al., 2013; Van de Waal et al., 2015; Kremp et al., 2019), even though cell quotas of 66 pg cell^{-1} (Tillmann et al., 2014) and 85 pg cell^{-1} (John et al., 2001) have also been reported. Strain W4-B9 had relatively low PST cell quotas of 4–16 pg cell^{-1} compared to cell quotas of up to 90 pg cell^{-1} reported from The Netherlands (Martens et al., 2016, 2017) or up to 280 pg cell^{-1} in strains from Chile (Salgado et al., 2015). However, strain W4-B9 is in range of other strains from the Baltic Sea, with cell quotas between 1 and 10 pg cell^{-1} (Suikkanen et al., 2013). During the experiments, CI cell quotas of strain 4-F7 were relatively stable, while 2-fold and 3-fold, and 4-fold changes in toxin cell quotas were observed in strains 4-C4 and K2-A8, and W4-B9, respectively. Changes in toxin cell quota in connection with different environmental conditions have often been reported, but bottom-up factors are suggested to only influence different growth parameters that in turn affect toxin cell quota (Parkhill and Cembella, 1999). Among these parameters, a negative correlation between growth rate and toxin cell quota was suggested (Sala-Pérez et al., 2016), and this connection has been detected for strains K2-A8 and 4-C4. In addition, a negative correlation between cell density and toxin cell quota has been described (Medhioub et al., 2011) that was detected in all strains of the present study, excluding strain 4-F7. Furthermore, Martens et al. (2016) suggested a positive correlation between cell volume and toxin cell quota that was present in all strains in the present study. The multitude of connections between different growth parameters and toxin cell quota, together with different responses of the four strains show the complex connection between environmental factors and toxin cell quota. In addition, these findings show that the effects of toxic harmful algal blooms cannot solely be determined by the cell density of the causative organism.

4.3. Toxin composition and novel cyclic imines

While toxin cell quotas were subject to variation during the experiments, the qualitative toxin compositions of all strains were stable. A broad variety of CI composition of *A. ostenfeldii* from a limited geographic area has been described for the east coast of Canada (Qiu et al., 2018) and also for a blooming event in The Netherlands (Martens et al., 2017), suggesting that environmental factors alone do not determine the toxin profile of *A. ostenfeldii*.

The two strains, 4-C4 and 4-F7 from the Kongsfjord produced exclusively CI, and mostly SPX C and 20-methyl-SPX G, two compounds that differ in their trispiroketal ring system (Nieva et al., 2020). Both toxins have a high toxicity in mice (Munday et al., 2012), and both compounds have been described in multiple strains isolated at the west coast of Greenland (Tillmann et al., 2014). Furthermore, the dominance of SPX C and 20-methyl-SPX G in the two strains from the Kongsfjord may indicate their origin, as the latter is found in *A. ostenfeldii* populations across the entire North Atlantic, SPX C is rarely found outside the Northwest Atlantic (Kremp et al., 2014; Tillmann et al., 2014; Qiu et al., 2018). From a chemotaxonomic perspective, the origin of the Kongsfjord strains - despite of the geographic proximity of Svalbard and Europe - seems to be the Northwest Atlantic rather than the East Atlantic.

Additionally, both strains produce the yet unreported spirolides provisionally named compounds 1–5. Of these compounds, Cp1 and Cp2 have a typical fragmentation pattern of C-type spirolides with a 5:5:6 tricyclic system, consisting of up to four water losses, the group 1 fragments in the range of *m/z* 400–500, and the cyclic imine fragment of *m/z* 164 or 180 (Figure S5h,i) (Sleno et al., 2004a, 2004b). Cp1 had an exact mass of *m/z* of 690.4722 ($C_{43}H_{64}NO_6$), and unit mass spectrum would suggest the structure of SPX 1 with an additional unsaturation (double bond). However, high mass resolution of fragment *m/z* 442 of the CID spectrum revealed that the mass difference of 2 Da between SPX 1 and Cp1 resulted from a missing hydroxy group (−16 *m/z*) of SPX 1 and an additional methyl group (+14 *m/z*). Characteristic fragments of C-type spirolides, like *m/z* 164, 206 and 258, were detected in both Cp1 and SPX C (Figure S5e,h), suggesting that both SPX share the structural element C_{23} to C_{35} (see Figure S6a for the position of C_{23} to C_{35}). While SPX C forms fragments *m/z* 476, 458, and 440, Cp1 formed fragments with *m/z* 460, 442, 424, which are reduced by 16 *m/z* in comparison to SPX C, suggesting that the loss of the hydroxy group must have occurred in the tricyclic system between C_{12} and C_{22}. With the only hydroxy group present in SPX C is located at C_{19}, we propose that Cp1 is 19-deshydroxy-SPX C (Figure S6a).

Cp2 has an exact mass of *m/z* 722.4625 ($C_{43}H_{64}NO_8$) and the most obvious difference of its CID spectrum in comparison to the spectra of most spirolides is the upshift of the cycloimine fragment of *m/z* 164 by 16 m/z to 180 (Figure S5j). This fragment has been reported to be indicative of an additional hydroxy group at C_{27} (Ciminiello et al., 2010). While 27-hydroxy-13-desmethyl-SPX C has a *m/z* of 708, Cp2 has a *m/z* of 722, meaning an increase of 14 *m/z*, suggesting a methyl group at C_{13} that is common in C-type spirolides. Therefore, the CID spectrum and high-resolution mass data of Cp2 are consistent with the chemical structure of 27-hydroxy-SPX C (Figure S6b). This compound has already been described from other *A. ostenfeldii* strains from the Arctic (Tillmann et al., 2014), but its unambiguous structural confirmation by nuclear magnetic resonance (NMR) spectroscopy is still lacking.

The CID spectrum of Cp3 (Figure S5j) also has a typical pattern of C-type SPXs characterized by the 5:5:6 tricyclic system. The accurate mass of Cp3 was determined as *m/z* 710.4623 corresponding to an elemental composition of $C_{42}H_{64}NO_8$. The fragments *m/z* 164, 206, 220, 230, 342, and 458 indicate that the structural element including C_{13} to C_{33} of Cp3 and SPX C are identical. However, comparison of the elemental compositions of Cp3 ($C_{42}H_{64}NO_8$) and SPX C ($C_{43}H_{64}NO_7$) reveals that Cp3 contains one carbon atom less and one additional oxygen atom compared to SPX C. As Cp3 and SPX C share the structural element C_{13} - C_{33}, the differences must be localized in the C_2 - C_{11} part of the molecule. As differences in C-composition of SPX are usually caused by varying numbers of methylations, it is reasonable to assume that Cp3 has methyl group less than SPX C and an additional hydroxylation in the C_2 - C_{11} part. In addition, in the same part of the molecule a saturation of a double bond is needed to match the chemical composition and the *m/z*

of 710 (Figure S6c). Without a complete structural elucidation by NMR, the exact structure of Cp3 remains unknown. Nevertheless, the missing double bond can only be located between C_2 and C_3 or between C_8 and C_9, as the double bond between C_5 and C_6 is necessary for the retro Diels-Alder reaction resulting in the opening of the macrocycle, which in turn is necessary for the observed fragmentations. A saturation of the double bond between C_8 and C_9 would define Cp3 as a C-type SPX, whereas saturated double bond at C_2/C_3 would define Cp3 as a d-type SPX (Hu et al., 1995).

In contrast to Cp1, 2, and 3, Cp4 and Cp5 most likely belong to the G-type SPX, with a 5:6:6 tricyclic ring system. The change from a 5:5:6 to a 5:6:6 tricyclic ring assembly results in a different fragmentation of the tricyclic ring assembly leading to the formation of fragments in the *m/z* 300–400 range (Aasen et al., 2005) that are completely absent in C-type SPX (Fig. S4 k, l), which makes G-type SPXs easy to identify. Cp4 has an exact mass *m/z* 720.4836 ($C_{44}H_{66}NO_7$) and in addition to three water losses, forms fragments *m/z* 472, 452, 376, 346, and 164 (Figure S5k). An identical spectrum has been recorded for an unknown SPX from an *A. ostenfeldii* strain from Norway and it has been suggested to be SPX C with an additional methyl group (Aasen et al., 2005). However, the same spectrum was reported for *A. ostenfeldii* from the west coast of Greenland, and it has been suggested to be a G-type SPX with an additional hydroxy group at C_{10}, a lacking hydroxy group at C_{17}, and an additional methyl group at C_{13} and C_{20} each (Nieva et al., 2020). However, NMR analysis is necessary to completely elucidate the structure of Cp4.

Cp5 had an accurate mass of *m/z* 722.4625 ($C_{43}H_{64}NO_8$) and its fragmentation resulted in an intense fragment of *m/z* 180 (Figure S5l), suggesting a hydroxylation at C27 as in 27-hydroxy-SPX C (Cp2). All recorded fragments had a *m/z* 16 higher mass than fragments of 20-methyl-SPX G, suggesting that Cp5 is 28-hydroxy-20-methyl-SPX G, an analogue of 20-methyl-SPX G with the additional hydroxy group at C_{28}, which corresponds to the same position of C_{27} in C-type SPXs, as the 5:6:6 trispiroketal ring systems causes a shift of the numeration of C-atoms (Figure S6d).

While the CI produced by the two arctic strains are diverse, none of the tested *A. ostenfeldii* from the Kongsfjord were found to produce PSTs, and identical results have been obtained for *A. ostenfeldii* strains isolated at the west coast of Greenland, (Tillmann et al., 2014). Yet, PSTs have been found in field samples from the Arctic, but are thus probably only produced by *Alexandrium catenella* (Tillmann et al., 2016; Rodríguez-Marconi et al., 2024).

In contrast to the strains from the Kongsfjord, strain K2-A8 from Kiel produced mostly SPX 1 and 13,19-didesmethyl-SPX C-two nearly identical compounds (Hu et al., 2001; Ciminiello et al., 2007) that are also highly toxic in mice (Munday et al., 2012; Finch et al., 2024). A similar toxin profile has been reported for a strain from the Kattegat (Otero et al., 2010), where 13,19-didesmethyl-SPX C was the major compound, but strains from the nearby Limfjord produced mainly SPX G or GYM A (Kremp et al., 2019). Furthermore, strain K2-A8 produced different

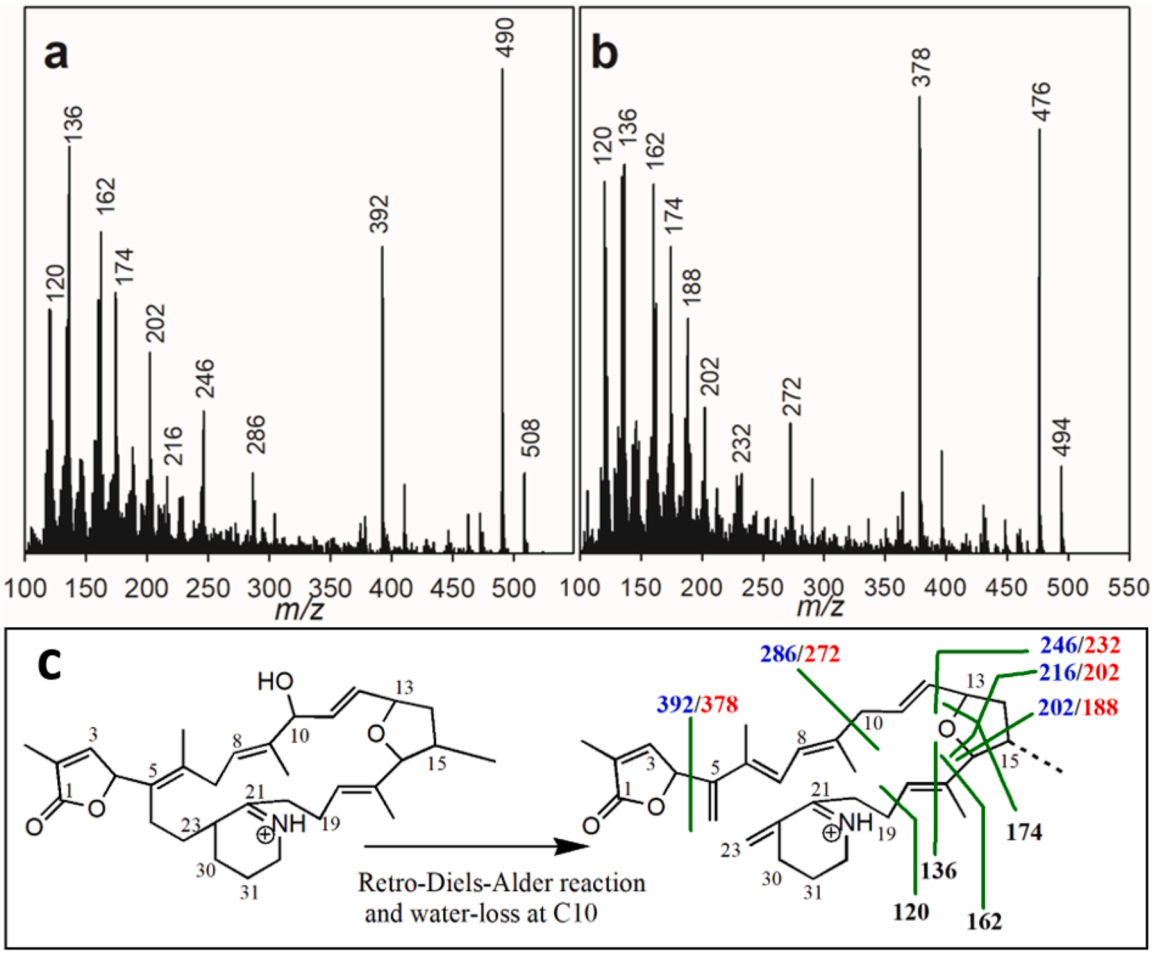

Fig. 9. a) CID spectrum of gymnodimine A; b) CID spectrum of 15-desmethyl-gymnodimine A with fragments above *m/z* 174 reduced by 14 in comparison to gymnodimine A; c) Chemical structure of gymnodimine A and CID fragmentation pattern according to Van Wagoner et al. (2011) and Varriale et al. (2021). Cleavages are highlighted in green. Bold number show *m/z* of fragments. Black numbers indicate fragments that occur in both, gymnodimine A and desmethyl-gymnodimine A, blue number show *m/z* of fragments occurring in gymnodimine A, and red numbers indicate fragments that are solely formed from the fragmentation of 15-desmethyl-gymnodimine A. The dotted methyl group at C15 indicates the missing methyl group in 15-desmethyl-gymnodimine A.

minor compounds (Table 2, Figure S2) among them, to our best knowledge, for the first time 15-desmethyl-gymnodimine A was described. 15-desmethyl-gymnodimine A has a *m/z* of 494, a downshift of 14 compared to GYM A. CID spectra of both compounds are identical in the range from *m/z* 120 to 174 Fig. 9a,b). Following the fragmentation pattern of gymnodimines (Van Wagoner et al., 2011; Varriale et al., 2021), these findings suggest that both molecules share the same structure between C_{16} and C_{21} (Fig. 9c). However, fragments with an *m/z* above 174 differ between compounds. While the CID of GYM A produces fragments of *m/z* 202, 216, 246, 286, 392, and 490, fragments of desmethyl-gymnodimine A always have *m/z* reduced by 14, suggesting the loss of a methyl group at C_{15} (Fig. 9).

While the two arctic strains had identical toxin profiles, the two strains from the Baltic Sea strongly differed in their toxin profile, with only strain W4-B9 producing PSTs and strain K2-A8 producing only CI. Generally, the PST composition of *A. ostenfeldii* is diverse and different PST profiles have been reported. With a profile consisting of STX, GTX-2/3, B1 and C1/C2, strain W4-B9 confers with strains from a brackish creek in The Netherlands (Van de Waal et al., 2015), and also with strains from the north-west Atlantic (Borkman et al., 2012; Tomas et al., 2012), but in contrast to strain W4-B9, the strains from The Netherlands and from the north-west Atlantic additionally produce CIs. On the other hand, the PST profile of strain W4-B9 differs from northern Baltic Sea *A. ostenfeldii* which lack B1 and C1/C2 toxins (Kremp et al., 2009; Riobó et al., 2013), and from the profile of a strain from the Öresund that is solely composed of GTX2/3 and STX (Kremp et al., 2014). These differences suggest a differentiation between populations on the level of toxin profiles, as PST profiles seem to be stable on a smaller geographical scale. For example, from a blooming event in The Netherlands, 68 strains of *A. ostenfeldii* have been described with identical PST profiles (Martens et al., 2017), and 88 strains of *Alexandrium catenella* from the Scottish North Sea showed a consistent presence of STX and C1/C2 toxins (Alpermann et al., 2010). As a response to higher temperatures, the STX ratio of strain W4-B9 increased by 18 % at 27 °C compared to 15 °C while the ratio of C1/C2 decreased. As STX is the most potent of PST and the C-toxins the least potent (Wiese et al., 2010), this shift of ratios increased the total cellular toxicity of this strain by 20 %. The same shift, yet less distinct, was also observed at high salinities, which is contrary to a study on an *A. ostenfeldii* strain from The Netherlands with an increase of STX at low salinities (Martens et al., 2016). However, the less potent C-toxins can be transformed to more potent GTX in different species of shellfish (Jaime et al., 2007), which make it difficult to assess how changes in the toxin profile of *A. ostenfeldii* affect the actual significant toxicity effects on humans or the environment. However, the distribution of PST- and CI-producing *A. ostenfeldii* in the Baltic Sea and areas where both populations overlap should be of interest in future field campaigns studying the distribution of phycotoxins.

5. Conclusions

The present study revealed strong intraspecific variability in four strains of *A. ostenfeldii* isolated from different regions, but also on a smaller geographic scale, between two strains from the Baltic Sea. The results propose that arctic strains will possibly benefit from climate change and increasing temperatures, supporting faster growth. The two strains from the Baltic Sea showed distinct differences in their growth response to salinities and temperatures, suggesting that increasing temperatures can be beneficial for strain W4-B9, but not for strain K2-A8. This might lead to an increase in PST producing *A. ostenfeldii* populations in the southern Baltic Sea. Furthermore, the present study shows the complex network of parameters that influence the toxin quotas of the four tested strains. Whether toxin quotas are directly influenced by environmental regimes or indirectly by physiological growth parameters remains uncertain. In this study, the toxin composition of strain W4-B9 showed an increase in STX and a decrease of C1/C2-toxins at higher temperatures, leading to a higher cellular toxicity. Furthermore, *A. ostenfeldii* was identified as a producer of desmethyl-gymnodimine A and novel spirolides were described from arctic *A. ostenfeldii*. However, further research is necessary on the toxicity of novel compounds.

Funding

S.T. was funded by the German Federal Ministry of Education and Research (BMBF), grant number 01LP2007A to B.K. and U.T.

CRediT authorship contribution statement

Simon Tulatz: Writing – original draft, Investigation, Visualization, Conceptualization, Methodology. **Urban Tillmann:** Writing – review & editing, Investigation, Resources, Funding acquisition, Supervision, Methodology, Conceptualization. **Bernd Krock:** Writing – review & editing, Resources, Investigation, Methodology, Conceptualization, Supervision, Funding acquisition. **Jan Tebben:** Writing – review & editing, Investigation. **Cédric Leo Meunier:** Writing – review & editing, Conceptualization, Supervision.

Declaration of competing interest

The authors declare that they have no known competing financial interests or personal relationships that could have appeared to influence the work reported in this paper.

Acknowledgement

We want to thank Annegret Müller and Thomas Max for their help with toxin analysis and various technical assistance. Furthermore, we thank the AWIPEV on-site staff Fieke Rader, Apolline Pibarot, Mathilde Carbonnel, and Guillaume Herment for their diverse assistance while sampling in the Kongsfjord.

Supplementary materials

Supplementary material associated with this article can be found, in the online version, at doi:10.1016/j.hal.2025.102918.

Data availability

Data will be made available on request.

References

Aasen, J., MacKinnon, S.L., LeBlanc, P., Walter, J.A., Hovgaard, P., Aune, T., Quilliam, M.A., 2005. Detection and identification of spirolides in Norwegian shellfish and plankton. Chem. Res. Toxicol 18, 509–515. https://doi.org/10.1021/tx049706n.

Almandoz, G.O., Montoya, N.G., Hernando, M.P., Benavides, H.R., Carignan, M.O., Ferrario, M.E., 2014. Toxic strains of the *alexandrium ostenfeldii* complex in southern South America (Beagle Channel, Argentina). Harmful Algae 37, 100–109. https://doi.org/10.1016/j.hal.2014.05.011.

Alpermann, T.J., Tillmann, U., Beszteri, B., Cembella, A.D., John, U., 2010. Phenotypic variation and genotypic diversity in a planktonic population of the toxigenic marine dinoflagellate *Alexandrium tamarense* (Dinophyceae). J. Phycol 46, 18–32. https://doi.org/10.1111/j.1529-8817.2009.00767.x.

Anderson, D.M., Andersen, P., Bricelj, V.M., Cullen, J.J., Rensel, J.E.J., 2001. Monitoring and management strategies for harmful algal blooms in coastal waters. Asia Pac. Econ. Program Singap., Intergov, Ocean., Comm, Tech. Ser. No. 59, Paris.

Anderson, D.M., Alpermann, T.J., Cembella, A.D., Collos, Y., Masseret, E., Montresor, M., 2012. The globally distributed genus *Alexandrium*: multifaceted roles in marine ecosystems and impacts on human health. Harmful Algae 14, 10–35. https://doi.org/10.1016/j.hal.2011.10.012.

Anderson, D.M., Fachon, E., Pickart, R.S., Lin, P., Fischer, A.D., Richlen, M.L., Uva, V., Brosnahan, M.L., McRaven, L., Bahr, F., Lefebvre, K., Grebmeier, J.M., Danielson, S. L., Lyu, Y., Fukai, Y., 2021. Evidence for massive and recurrent toxic blooms of *alexandrium catenella* in the Alaskan Arctic. Proc, Natl, Acad, Sci, U. S. A 118. https://doi.org/10.1073/pnas.2107387118.

Andersson, A., Meier, H.E.M., Ripszam, M., Rowe, O., Wikner, J., Haglund, P., Eilola, K., Legrand, C., Figueroa, D., Paczkowska, J., Lindehoff, E., Tysklind, M., Elmgren, R.,

2015. Projected future climate change and Baltic Sea ecosystem management. Ambio 44, 345–356. https://doi.org/10.1007/s13280-015-0654-8.
Bhaskar, J.T., Parli, B.V., Tripathy, S.C., 2020. Spatial and seasonal variations of dinoflagellates and ciliates in the Kongsfjorden. Svalbard, Mar, Ecol 41, 1–12. https://doi.org/10.1111/maec.12588.
Borkman, D.G., Smayda, T.J., Tomas, C.R., York, R., Strangman, W., Wright, J.L.C., 2012. Toxic *alexandrium peruvianum* (Balech and de Mendiola) balech and Tangen in Narragansett Bay, Rhode Island (USA). Harmful Algae 19, 92–100. https://doi.org/10.1016/j.hal.2012.06.004.
Boyd, P.W., Rynearson, T.A., Armstrong, E.A., Fu, F., Hayashi, K., Hu, Z., Hutchins, D.A., Kudela, R.M., Litchman, E., Mulholland, M.R., Passow, U., Strzepek, R.F., Whittaker, K.A., Yu, E., Thomas, M.K., 2013. Marine Phytoplankton temperature versus growth responses from polar to tropical waters - outcome of a scientific community-wide study. PLoS One 8. https://doi.org/10.1371/journal.pone.0063091.
Brandenburg, K.M., de Senerpont Domis, L.N., Wohlrab, S., Krock, B., John, U., van Scheppingen, Y., van Donk, E., Van de Waal, D.B., 2017. Combined physical, chemical and biological factors shape *alexandrium ostenfeldii* blooms in The Netherlands. Harmful Algae 63, 146–153. https://doi.org/10.1016/j.hal.2017.02.004.
Brandenburg, K.M., Krock, B., Klip, H.C.L., Sluijs, A., Garbeva, P., Van de Waal, D.B., 2021. Intraspecific variation in multiple trait responses of *alexandrium ostenfeldii* towards elevated pCO2. Harmful Algae 101, 101970. https://doi.org/10.1016/j.hal.2020.101970.
Caroppo, C., Pagliara, P., Azzaro, F., Miserocchi, S., Azzaro, M., 2017. Late summer phytoplankton blooms in the changing polar environment of the Kongsfjorden (Svalbard, Arctic). Cryptogam, Algol 38, 53–72. https://doi.org/10.7872/crya/v38.iss1.2017.53.
Cembella, A.D., Lewis, N.I., Quilliam, M.A., 2000. The marine dinoflagellate *Alexandrium ostenfeldii* (Dinophyceae) as the causative organism of spirolide shellfish toxins. Phycologia 39, 67–74. https://doi.org/10.2216/i0031-8884-39-1-67.1.
Ching, P.K., Ramos, R.A., de los Reyes, V.C., Sucaldito, M.N., Tayag, E., 2015. Lethal paralytic shellfish poisoning from consumption of green mussel broth, Western Samar, Philippines, August 2013. West, Pac. Surveill, response J. WPSAR 6, 22–26. https://doi.org/10.5365/WPSAR.2015.6.1.004.
Ciminiello, P., Dell'Aversano, C., Fattorusso, E., Magno, S., Tartaglione, L., Cangini, M., Pompei, M., Guerrini, F., Boni, L., Pistocchi, R., 2006. Toxin profile of *alexandrium ostenfeldii* (Dinophyceae) from the Northern Adriatic Sea revealed by liquid chromatography-mass spectrometry. Toxicon 47, 597–604. https://doi.org/10.1016/j.toxicon.2006.02.003.
Ciminiello, P., Dell'Aversano, C., Fattorusso, E., Forino, M., Grauso, L., Tartaglione, L., Guerrini, F., Pistocchi, R., 2007. Spirolide toxin profile of adriatic *alexandrium ostenfeldii* cultures and structure elucidation of 27-hydroxy-13,19-didesmethyl spirolide C. J. Nat, Prod 70, 1878–1883. https://doi.org/10.1021/np0703242.
Ciminiello, P., Dell'Aversano, C., Iacovo, E.Dello, Fattorusso, E., Forino, M., Grauso, L., Tartaglione, L., Guerrini, F., Pezzolesi, L., Pistocchi, R., 2010. Characterization of 27-hydroxy-13-desmethyl spirolide C and 27-oxo-13,19-didesmethyl spirolide C. Further insights into the complex Adriatic *Alexandrium ostenfeldii* toxin profile. Toxicon 56, 1327–1333. https://doi.org/10.1016/j.toxicon.2010.07.016.
Feistel, R., Weinreben, S., Wolf, H., Seitz, S., Spitzer, P., Adel, B., Nausch, G., Schneider, B., Wright, D.G., 2010. Density and absolute salinity of the Baltic Sea 2006-2009. Ocean Sci 6, 3–24.
Finch, S.C., Harwood, D.T., Boundy, M.J., Selwood, A.I., 2024. A review of cyclic imines in shellfish: worldwide occurrence, toxicity and assessment of the risk to consumers. Mar. Drugs 22, 1–18. https://doi.org/10.3390/md22030129.
Fischer, P., Lienkämper, M., Schwanitz, M., Brix, H., 2024. Dataset: hydrographical time series data of the littoral zone of Kongsfjorden, Svalbard 2023. Pangaea. https://doi.org/10.1594/PANGAEA.967739.
Gobler, C.J., Doherty, O.M., Hattenrath-Lehmann, T.K., Griffith, A.W., Kang, Y., Litaker, R.W., 2017. Ocean warming since 1982 has expanded the niche of toxic algal blooms in the North Atlantic and North Pacific oceans. Proc, Natl, Acad, Sci, U. S. A 114, 4975–4980. https://doi.org/10.1073/pnas.1619575114.
Gräwe, U., Friedland, R., Burchard, H., 2013. The future of the western Baltic Sea: two possible scenarios. Ocean Dyn 63, 901–921. https://doi.org/10.1007/s10236-013-0634-0.
Gribble, K.E., Keafer, B.A., Quilliam, M.A., Cembella, A.D., Kulis, D.M., Manahan, A., Anderson, D.M., 2005. Distribution and toxicity of *Alexandrium ostenfeldii* (Dinophyceae) in the Gulf of Maine, USA. Deep. Res. Part II Top. Stud. Oceanogr. 52, 2745–2763. https://doi.org/10.1016/j.dsr2.2005.06.018.
Gromisz, S., Witek, Z., 2001. Main Phytoplankton assemblages in the Gulf of Gdansk and the Pomeranian Bay from 1994 to1997. Bull, Sea Fish, Inst 2, 31–51.
Gu, H., Zeng, N., Liu, T., Yang, W., Müller, A., Krock, B., 2013. Morphology, toxicity, and phylogeny of *alexandrium* (Dinophyceae) species along the coast of China. Harmful Algae 27, 68–81. https://doi.org/10.1016/j.hal.2013.05.008.
Guinder, V.A., Tillmann, U., Krock, B., Delgado, A.L., Krohn, T., Cardona, J.E.G., Metfies, K., Abbate, C.L., Silva, R., Lara, R., 2018. Plankton multiproxy analyses in the Northern Patagonian Shelf, Argentina: community structure, phycotoxins, and characterization of toxic *Alexandrium* strains. Front, Mar, Sci 5, 1–21. https://doi.org/10.3389/fmars.2018.00394.
Guindon, S., Dufayard, J.F., Lefort, V., Anisimova, M., Hordijk, W., Gascuel, O., 2010. New algorithms and methods to estimate maximum-likelihood phylogenies: assessing the performance of PhyML 3.0. Syst, Biol 59, 307–321. https://doi.org/10.1093/sysbio/syq010.
Hajdu, S., Edler, L., Olenina, I., Witek, B., 2000. Spreading and establishment of the potentially toxic dinoflagellate *prorocentrum minimum* in the Baltic Sea. Int, Rev, Hydrobiol 85, 561–575. https://doi.org/10.1002/1522-2632(200011)85:5/6<561::AID−IROH561>3.0.CO;2-3.
Hakanen, P., Suikkanen, S., Franzén, J., Franzén, H., Kankaanpää, H., Kremp, A., 2012. Bloom and toxin dynamics of *alexandrium ostenfeldii* in a shallow embayment at the SW coast of Finland, northern Baltic Sea. Harmful Algae 15, 91–99. https://doi.org/10.1016/j.hal.2011.12.002.
Hällfors, H., Backer, H., Leppänen, J.M., Hällfors, S., Hällfors, G., Kuosa, H., 2013. The northern Baltic Sea phytoplankton communities in 1903-1911 and 1993-2005: a comparison of historical and modern species data. Hydrobiologia 707, 109–133. https://doi.org/10.1007/s10750-012-1414-4.
Hansen, P.J., Cembella, A.D., Moestrup, Ø., 1992. The Marine Dinoflagellate *Alexandrium ostenfeldii*: paralytic shellfish toxin concentration, composition, and toxicity to a tintinnid ciliate. J. Phycol 28, 597–603.
Hasle, G.R., Heimdal, B.R., 1998. The net phytoplankton in Kongsfjorden, Svalbard, July 1988, with general remarks on species composition of Arctic phytoplankton. Polar Res 17, 31–52. https://doi.org/10.3402/polar.v17i1.6605.
Hu, T., Curtis, J.M., Oshima, Y., Quilliam, M.A., Walter, J.A., Wendy, M., Wright, J.L.C., 1995. Spirolides B and D, two novel macrocycles isolated from the digestive glands of shellfish. J. Chem, Sosciety Chem, Commun.
Hu, T., Burton, I.W., Cembella, A.D., Curtis, J.M., Quilliam, M.A., Walter, J.A., Wright, J. L.C., 2001. Characterization of spirolides A, C, and 13-desmethyl C, new marine toxins isolated from toxic plankton and contaminated shellfish. J. Nat, Prod 64, 308–312. https://doi.org/10.1021/np000416q.
Jaime, E., Gerdts, G., Luckas, B., 2007. In vitro transformation of PSP toxins by different shellfish tissues. Harmful Algae 6, 308–316. https://doi.org/10.1016/j.hal.2006.04.003.
Jensen, M.Ø., Moestrup, Ø., 1997. Autecology of the toxic dinoflagellate *alexandrium ostenfeldii*: life history and growth at different temperatures and salinities. Eur, J. Phycol 32, 9–18. https://doi.org/10.1080/09541449710001719325.
John, U., Quilliam, M.A., Medlin, L., Cembella, A.D., 2001. Spirolide production and photoperiod-dependent growth of the marine dinoflagellate *alexandrium ostenfeldii*. In: Hallegraeff, G.M., Blackburn, S.I., Bolch, C.J., Lewis, R.J. (Eds.), Harmful Algal Blooms 2000. Intergovernmental Oceanographic Commission of UNESCO, Paris, pp. 299–301, 2001.
Karcher, M., Beszczynska-Möller, A., Kauker, F., Gerdes, R., Heyen, S., Rudels, B., Schauer, U., 2011. Arctic Ocean warming and its consequences for the Denmark Strait overflow. J. Geophys, Res, Ocean 116, 1–10. https://doi.org/10.1029/2010JC006265.
Keller, M.D., Selvin, R.C., Guillard, R.R.L., Claus, W., 1987. Media for the Culture of Oceanic Ultraphytoplankton. J. Phycol 23, 633–638.
Kim, H., Park, H., Wang, H., Yoo, H.Y., Park, J., Ki, J.S., 2021. Low temperature and cold stress significantly increase saxitoxins (Stxs) and expression of stx biosynthesis genes sxta4 and sxtg in the dinoflagellate Alexandrium catenella. Mar. Drugs 19. https://doi.org/10.3390/md19060291.
Kim, Jin Ho, Park, B.S., Kim, Joo Hwan, Wang, P., Han, M.S., 2015. Intraspecific diversity and distribution of the cosmopolitan species *Pseudo-nitzschia pungens* (Bacillariophyceae): morphology, genetics, and ecophysiology of the three clades. J. Phycol 51, 159–172. https://doi.org/10.1111/jpy.12263.
Kremp, A., Lindholm, T., Dreßler, N., Erler, K., Gerdts, G., Eirtovaara, S., Leskinen, E., 2009. Bloom forming *alexandrium ostenfeldii* (Dinophyceae) in shallow waters of the Åland Archipelago, Northern Baltic Sea. Harmful Algae 8, 318–328. https://doi.org/10.1016/j.hal.2008.07.004.
Kremp, A., Tahvanainen, P., Litaker, W., Krock, B., Suikkanen, S., Leaw, C.P., Tomas, C., 2014. Phylogenetic relationships, morphological variation, and toxin patterns in the *Alexandrium ostenfeldii* (Dinophyceae) complex: implications for species boundaries and identities. J. Phycol 50, 81–100. https://doi.org/10.1111/jpy.12134.
Kremp, A., Hansen, P.J., Tillmann, U., Savela, H., Suikkanen, S., Voß, D., Barrera, F., Jakobsen, H.H., Krock, B., 2019. Distributions of three Alexandrium species and their toxins across a salinity gradient suggest an increasing impact of GDA producing *A. pseudogonyaulax* in shallow brackish waters of Northern Europe. Harmful Algae 87, 101622. https://doi.org/10.1016/j.hal.2019.101622.
Krock, B., Seguel, C.G., Cembella, A.D., 2007. Toxin profile of *alexandrium catenella* from the Chilean coast as determined by liquid chromatography with fluorescence detection and liquid chromatography coupled with tandem mass spectrometry. Harmful Algae 6, 734–744. https://doi.org/10.1016/j.hal.2007.02.005.
Laabir, M., Collos, Y., Masseret, E., Grzebyk, D., Abadie, E., Savar, V., Sibat, M., Amzil, Z., 2013. Influence of environmental factors on the paralytic shellfish toxin content and profile of Alexandrium catenella (Dinophyceae) isolated from the Mediterranean Sea. Mar. Drugs 11, 1583–1601. https://doi.org/10.3390/md11051583.
Lim, P.T., Ogata, T., 2005. Salinity effect on growth and toxin production of four tropical *Alexandrium* species (Dinophyceae). Toxicon 45, 699–710. https://doi.org/10.1016/j.toxicon.2005.01.007.
Lovejoy, C., Vincent, W.F., Bonilla, S., Roy, S., Martineau, M.J., Terrado, R., Potvin, M., Massana, R., Pedrós-Alió, C., 2007. Distribution, phylogeny, and growth of cold-adapted picoprasinophytes in arctic seas. J. Phycol 43, 78–89. https://doi.org/10.1111/j.1529-8817.2006.00310.x.
Maclean, C., Cembella, A.D., Quilliam, M.A., 2003. Effects of light, salinity and inorganic nitrogen on cell growth and spirolide production in the marine dinoflagellate *alexandrium ostenfeldii* (Paulsen) balech et tangen. Bot, Mar 46, 466–476.
Martens, H., Van De Waal, D.B., Brandenburg, K.M., Krock, B., Tillmann, U., 2016. Salinity effects on growth and toxin production in an *alexandrium ostenfeldii* (Dinophyceae) isolate from The Netherlands. J. Plankton Res 38, 1302–1316. https://doi.org/10.1093/plankt/fbw053.
Martens, H., Tillmann, U., Harju, K., Dell'aversano, C., Tartaglione, L., Krock, B., 2017. Toxin variability estimations of 68 *Alexandrium ostenfeldii* (Dinophyceae) strains

from The netherlands reveal a novel abundant gymnodimine. Microorganisms 5. https://doi.org/10.3390/microorganisms5020029.
Medhioub, W., Sechet, V., Truquet, P., Bardouil, M., Amzil, Z., Lassus, P., Soudant, P., 2011. *Alexandrium ostenfeldii* growth and spirolide production in batch culture and photobioreactor. Harmful Algae 10, 794–803. https://doi.org/10.1016/j.hal.2011.06.012.
Moestrup, Ø., Hansen, P.J., 1988. On the occurrence of the potentially toxic dinoflagellates *Alexandrium tamarense* (= *Gonyaulax excavata*) and *A. ostenfeldii* in danish and faroese waters. Ophelia 28, 195–213. https://doi.org/10.1080/00785326.1988.10430813.
Möller, K., Thoms, S., Tillmann, U., Krock, B., Koch, F., Peeken, I., Meunier, C.L., 2024. Effects of bottom-up factors on growth and toxin content of a harmful algae bloom dinoflagellate. Limnol, Ocean. 69, 1335–1349. https://doi.org/10.1002/lno.12576.
Munday, R., Quilliam, M.A., LeBlanc, P., Lewis, N., Gallant, P., Sperker, S.A., Stephen Ewart, H., MacKinnon, S.L., 2012. Investigations into the toxicology of spirolides, a group of marine phycotoxins. Toxins (Basel) 4, 1–14. https://doi.org/10.3390/toxins4010001.
Neumann, T., 2010. Climate-change effects on the Baltic Sea ecosystem: a model study. J. Mar, Syst 81, 213–224. https://doi.org/10.1016/j.jmarsys.2009.12.001.
Nielsen, M.V., Tønseth, C.P., 1991. Temperature and salinity effect on growth and chemical composition of *gyrodinium aureolum* Hulburt in culture. J. Plankton Res 13, 389–398. https://doi.org/10.1093/plankt/13.2.389.
Nielsen, M.V., 1996. Growth and chemical composition of the toxic dinoflagellate *gymnodinium galatheanum* in relation to irradiance, temperature and salinity. Mar, Ecol, Prog, Ser 136, 205–211. https://doi.org/10.3354/meps136205.
Nieva, J.A., Tebben, J., Tillmann, U., Wohlrab, S., Krock, B., 2020. Mass spectrometry-based characterization of new spirolides from *Alexandrium ostenfeldii* (Dinophyceae). Mar. Drugs 18. https://doi.org/10.3390/md18100505.
Nordli, E., 1957. Experimental studies on the ecology of ceratia. Oikos 8, 200–265.
Ogata, T., Ishimaru, T., Kodama, M., 1987. Effect of Water temperature and light intensity on growth rate and toxicity change in Protogonyaulax tamarensis. Mar, Biol 95, 217–220.
Okolodkov, Y.B., Hapter, R., Semovski, S.V., 2000. Phytoplankton in kongsfjorden, spitsbergen, july 1996. Sarsia 85, 345–352. https://doi.org/10.1080/00364827.2000.10414585.
Omstedt, A., Axell, L.B., 2003. Modeling the variations of salinity and temperature in the large Gulfs of the Baltic Sea. Cont, Shelf Res 23, 265–294. https://doi.org/10.1016/S0278-4343(02)00207-8.
Otero, P.A.Z., Alfonso, A., Vieytes, M.R., Cabado, A.G., Vieites, J.M., Botana, L.M., 2010. Effects of environmental regimens on the toxin profile of *alexandrium ostenfeldii*. Env., Toxicol, Chem 29, 301–310. https://doi.org/10.1002/etc.41.
Pachauri, R.K., Allen, M.R., Barros, V.R., Broome, J., Cramer, W., Christ, R., Church, J.A., Clarke, L., Dahe, Q., Dasgupta, P., Dubash, N.K., Edenhofer, O., Elgizouli, I., Field, C. B., Forster, P., Friedlingstein, P., Fuglestvedt, J., Gomez-Echeverri, L., Hallegatte, S., Hegerl, G., Howden, M., Jiang, K., Cisneros, B.J., Kattsov, V., Lee, H., Mach, K.J., Marotzke, J., Mastrandrea, M.D., Meyer, L., Minx, J., Mulugetta, Y., O'Brien, K., Oppenheimer, M., Pereira, J.J., Pichs-Madruga, R., Plattner, G., Pörtner, H.O., Power, S.B., Preston, B., Ravindranath, N.H., Reisinger, A., Riahi, K., Rusticucci, M., Scholes, R., Seyboth, K., Sokona, Y., Stavins, R., Stocker, T.F., Tschakert, P., van Vuuren, D., van Ypersele, J., 2014. IPCC, 2014: Climate Change 2014: Synthesis Report. Contribution of Working Groups I, II and III to the Fifth Assessment Report of the Intergovernmental Panel On Climate Change. IPCC, Geneva, Switzerland. https://doi.org/10.1016/S0022-0248(00)00575-3.
Pančić, M., Hansen, P.J., Tammilehto, A., Lundholm, N., 2015. Resilience to temperature and pH changes in a future climate change scenario in six strains of the polar diatom *fragilariopsis cylindrus*. Biogeosciences 12, 4235–4244. https://doi.org/10.5194/bg-12-4235-2015.
Parkhill, J.P., Cembella, A.D., 1999. Effects of salinity, light and inorganic nitrogen on growth and toxigenicity of the marine dinoflagellate *alexandrium tamarense* from northeastern Canada. J. Plankton Res 21, 939–955. https://doi.org/10.1093/plankt/21.5.939.
Paulsen, O., 1904. Plankton-investigations in the waters round Iceland in 1903. Meddelelser fra Komm. Havunders. Ser, Plankton Kbh. 1, 1–40.
Qiu, J., Rafuse, C., Lewis, N.I., Li, A., Meng, F., Beach, D.G., McCarron, P., 2018. Screening of cyclic imine and paralytic shellfish toxins in isolates of the genus *Alexandrium* (Dinophyceae) from Atlantic Canada. Harmful Algae 77, 108–118. https://doi.org/10.1016/j.hal.2018.05.005.
Rantanen, M., Karpechko, A.Y., Lipponen, A., Nordling, K., Hyvärinen, O., Ruosteenoja, K., Vihma, T., Laaksonen, A., 2022. The Arctic has warmed nearly four times faster than the globe since 1979. Commun, Earth Env. 3, 1–10. https://doi.org/10.1038/s43247-022-00498-3.
Riobó, P., Rodriguez, F., Garrido, J.L., Franco, J.M., 2013. Toxin profiles of *A. ostenfeldii* and *A. peruvianum*. Comparison of two clonal strains with different light tolerance. Marine and freshwater toxins analysis. In: Proceedings of the Fourth Joint Symposium and AOAC Task Force Meeting, Baiona-Pontevedra, Spain, pp. 5–9.
Rodríguez-Marconi, S., Krock, B., Tillmann, U., Tillmann, A., Voß, D., Zielinski, O., Vásquez, M., Trefault, N., 2024. Diversity of eukaryote plankton and toxins along the West Kalaallit Nunaat (Greenland) coast. Front, Mar, Sci 11, 1–18. https://doi.org/10.3389/fmars.2024.1443389.
Ronquist, F., Teslenko, M., Van Der Mark, P., Ayres, D.L., Darling, A., Höhna, S., Larget, B., Liu, L., Suchard, M.A., Huelsenbeck, J.P., 2012. Mrbayes 3.2: efficient bayesian phylogenetic inference and model choice across a large model space. Syst, Biol 61, 539–542. https://doi.org/10.1093/sysbio/sys029.
Sala-Pérez, M., Alpermann, T.J., Krock, B., Tillmann, U., 2016. Growth and bioactive secondary metabolites of arctic *protoceratium reticulatum* (Dinophyceae). Harmful Algae 55, 85–96. https://doi.org/10.1016/j.hal.2016.02.004.
Salgado, P., Riobó, P., Rodríguez, F., Franco, J.M., Bravo, I., 2015. Differences in the toxin profiles of *Alexandrium ostenfeldii* (Dinophyceae) strains isolated from different geographic origins: evidence of paralytic toxin, spirolide, and gymnodimine. Toxicon 103, 85–98. https://doi.org/10.1016/j.toxicon.2015.06.015.
Sejr, M.K., Stedmon, C.A., Bendtsen, J., Abermann, J., Juul-Pedersen, T., Mortensen, J., Rysgaard, S., 2017. Evidence of local and regional freshening of Northeast Greenland coastal waters. Sci, Rep 7. https://doi.org/10.1038/s41598-017-10610-9.
Seuthe, L., Iversen, K.R., Narcy, F., 2011. Microbial processes in a high-latitude fjord (Kongsfjorden, Svalbard): II. Ciliates and dinoflagellates. Polar Biol 34, 751–766. https://doi.org/10.1007/s00300-010-0930-9.
Siegel, H., Gerth, M., Tschersich, G., 2006. Sea surface temperature development of the Baltic Sea in the period 1990-2004. Oceanologia 48, 119–131.
Sildever, S., Jerney, J., Kremp, A., Oikawa, H., Sakamoto, S., Yamaguchi, M., Baba, K., Mori, A., Fukui, T., Nonomura, T., Shinada, A., Kuroda, H., Kanno, N., Mackenzie, L., Anderson, D.M., Nagai, S., 2019. Genetic relatedness of a new Japanese isolates of *alexandrium ostenfeldii* bloom population with global isolates. Harmful Algae 84, 64–74. https://doi.org/10.1016/j.hal.2019.02.005.
Silva, M., Barreiro, A., Rodriguez, P., Otero, P., Azevedo, J., Alfonso, A., Botana, L.M., Vasconcelos, V., 2013. New invertebrate vectors for PST, spirolides and okadaic acid in the North Atlantic. Mar. Drugs 11, 1936–1960. https://doi.org/10.3390/md11061936.
Sjöqvist, C., Godhe, A., Jonsson, P.R., Sundqvist, L., Kremp, A., 2015. Local adaptation and oceanographic connectivity patterns explain genetic differentiation of a marine diatom across the North Sea-Baltic Sea salinity gradient. Mol, Ecol 24, 2871–2885. https://doi.org/10.1111/mec.13208.
Sleno, L., Chalmers, M.J., Volmer, D.A., 2004a. Structural study of spirolide marine toxins by mass spectrometry: part II. Mass spectrometric characterization of unknown spirolides and related compounds in a cultured phytoplankton extract. Anal, Bioanal, Chem 378, 977–986. https://doi.org/10.1007/s00216-003-2296-0.
Sleno, L., Windust, A.J., Volmer, D.A., 2004b. Structural study of spirolide marine toxins by mass spectrometry: part I. Fragmentation pathways of 13-desmethyl spirolide C by collision-induced dissociation and infrared multiphoton dissociation mass spectrometry. Anal, Bioanal, Chem 378, 969–976. https://doi.org/10.1007/s00216-003-2297-z.
Smoła, Z.T., Tatarek, A., Wiktor, J.M., Wiktor, J.M.W., Kubiszyn, A., Węsławski, J.M., 2017. Primary producers and production in Hornsund and Kongsfjorden - comparison of two fjord systems. Pol. Polar Res 38, 351–373. https://doi.org/10.1515/popore-2017-0013.
Suikkanen, S., Kremp, A., Hautala, H., Krock, B., 2013. Paralytic shellfish toxins or spirolides? The role of environmental and genetic factors in toxin production of the *Alexandrium ostenfeldii* complex. Harmful Algae 26, 52–59. https://doi.org/10.1016/j.hal.2013.04.001.
Suzuki, Y., Takahashi, M., 1995. Growth responses of several diatom species isolated from various environments to temperature. J. Phycol 31, 880–888.
Tahvanainen, P., Alpermann, T.J., Figueroa, R.I., John, U., Hakanen, P., Nagai, S., Blomster, J., Kremp, A., 2012. Patterns of post-glacial genetic differentiation in marginal populations of a marine microalga. PLoS One 7. https://doi.org/10.1371/journal.pone.0053602.
Tillmann, U., Kremp, A., Tahvanainen, P., Krock, B., 2014. Characterization of spirolide producing *alexandrium ostenfeldii* (Dinophyceae) from the western Arctic. Harmful Algae 39, 259–270. https://doi.org/10.1016/j.hal.2014.08.008.
Tillmann, U., Krock, B., Alpermann, T.J., Cembella, A., 2016. Bioactive compounds of marine dinoflagellate isolates from western Greenland and their phylogenetic association within the genus *Alexandrium*. Harmful Algae 51, 67–80. https://doi.org/10.1016/j.hal.2015.11.004.
Tillmann, U., Trefault, N., Krock, B., Parada-Pozo, G., De La Iglesia, R., Vásquez, M., 2017. Identification of *Azadinium poporum* (Dinophyceae) in the Southeast Pacific: morphology, molecular phylogeny, and azaspiracid profile characterization. J. Plankton Res 39, 350–367. https://doi.org/10.1093/plankt/fbw099.
Tillmann, U., Beran, A., Gottschling, M., Wietkamp, S., Hoppenrath, M., 2022. Clarifying confusion–*Prorocentrum triestinum* J.Schiller and *prorocentrum redfieldii* Bursa (Prorocentrales, Dinophyceae) are two different species. Eur, J. Phycol 57, 207–226. https://doi.org/10.1080/09670262.2021.1948614.
Tomas, C.R., van Wagoner, R., Tatters, A.O., White, K.D., Hall, S., Wright, J.L.C., 2012. *Alexandrium peruvianum* (Balech and Mendiola) Balech and Tangen a new toxic species for coastal North Carolina. Harmful Algae 17, 54–63. https://doi.org/10.1016/j.hal.2012.02.011.
Tulatz, S., Krock, B., Tillmann, U., Meunier, C.L., 2024. Effects of temperature, salinity and CO2 concentration on growth and toxin production of the harmful algal bloom species *alexandrium pseudogonyaulax* (Dinophyceae) from the Danish Limfjord. Harmful Algae 140. https://doi.org/10.1016/j.hal.2024.102756.
Väinölä, R., Hvilsom, M.M., 1991. Genetic divergence and a hybrid zone between Baltic and North Sea *Mytilus* populations (Mytilidae: mollusca). Biol, J. Linn, Soc 43, 127–148. https://doi.org/10.1111/j.1095-8312.1991.tb00589.x.
Van de Waal, D.B., Tillmann, U., Martens, H., Krock, B., van Scheppingen, Y., John, U., 2015. Characterization of multiple isolates from an *alexandrium ostenfeldii* bloom in The Netherlands. Harmful Algae 49, 94–104. https://doi.org/10.1016/j.hal.2015.08.002.
Van Wagoner, R.M., Misner, I., Tomas, C.R., Wright, J.L.C., 2011. Occurrence of 12-methylgymnodimine in a spirolide-producing dinoflagellate *alexandrium peruvianum* and the biogenetic implications. Tetrahedron Lett. 52, 4243–4246. https://doi.org/10.1016/j.tetlet.2011.05.137.
Varriale, F., Tartaglione, L., Cinti, S., Milandri, A., Dall'Ara, S., Calfapietra, A., Dell'Aversano, C., 2021. Development of a data dependent acquisition-based

approach for the identification of unknown fast-acting toxins and their ester metabolites. Talanta 224, 121842. https://doi.org/10.1016/j.talanta.2020.121842.

Wang, H., Kim, H., Park, H., Ki, J.S., 2022. Temperature influences the content and biosynthesis gene expression of saxitoxins (STXs) in the toxigenic dinoflagellate Alexandrium pacificum. Sci, Total Env. 802. https://doi.org/10.1016/j.scitotenv.2021.149801.

Wiese, M., D'Agostino, P.M., Mihali, T.K., Moffitt, M.C., Neilan, B.A., 2010. Neurotoxic alkaloids: saxitoxin and its analogs. Mar. Drugs 8, 2185–2211. https://doi.org/10.3390/md8072185.